


# Magnetic moment orientation and in-depth distribution of dysprosium near the surface of DyCo<sub>4,6</sub> thin films from x-ray circularly polarized absorption

J. Díaz<sup>✉\*</sup> and C. Blanco-Roldán

*Universidad de Oviedo, Calle Federico García Lorca, 18, Oviedo 33007, Spain  
and CINN (CSIC-Universidad de Oviedo), 33940 El Entrego, Spain*

 (Received 18 March 2021; revised 22 July 2021; accepted 5 August 2021; published 30 August 2021)

We have investigated the dysprosium distribution and its magnetic moment orientation at the region near the surface of DyCo<sub>4,4</sub> and DyCo<sub>4,6</sub> ferrimagnetic amorphous films with perpendicular magnetic anisotropy. X-ray magnetic circular dichroism spectroscopy of the films at the Dy  $M_{4,5}$  and Co  $L_{2,3}$  edges using total electron yield (TEY) detection was performed at 2 K and 300 K temperatures, and at sample orientations ranged from 0° to 70° with respect to the normal to the sample. The measurements showed an apparent partial decoupling between the cobalt and dysprosium magnetic sublattices. At RT, the magnetic moment per atom of dysprosium was below the minimum value expected if all dysprosium moments were Antiferromagnetic (AF) coupled to cobalt. At 2 K, the cobalt sublattice presented a surprisingly stronger magnetic anisotropy than the dysprosium sublattice. A detailed analysis of the circularly polarized spectra of the Dy  $M_5$  edge, based on the deconvolution of the spectra in their related parallel, antiparallel, and transverse to  $J_z$  spectral components, demonstrates that the spectra are composed by dysprosium with different magnetic moment distributions. The fit of the Dy  $M_5$  spectra using the  $J_z$  spectral components evidenced a gradation of dysprosium concentration due to segregation at the region probed by TEY. The topmost layer was magnetically uncoupled from cobalt. At RT, 25% of the dysprosium magnetic moments in the underlayer were found averaged oriented in the same direction of cobalt. The expected weak magnetic coupling of these dysprosium atoms to cobalt should explain the surprisingly lower magnetic anisotropy of the dysprosium sublattice compared to that of cobalt probed by TEY at 2 K.

DOI: [10.1103/PhysRevB.104.054439](https://doi.org/10.1103/PhysRevB.104.054439)

## I. INTRODUCTION

Rare earth-transition metal (RE-TM) alloys are well-known magnetic materials since decades ago [1,2], constituting a key component in a variety of industrial and technological applications. A renewed interest in these materials has grown because of their richness in magnetic behaviors and their relative flexibility for tailoring their properties to fit in specific magnetic applications and devices. RE-TM alloys are present in spring magnets [3–5], magnetic topological formations [6–8], spin-wave functional devices [9], and all optical magnetic switching [10–12]. Their use is also favored by its simple thin-film preparation process, which can be done at RT.

The extraordinary magnetic properties of these alloys are based on the strength of the TM-TM exchange coupling, the high magnetic moment of the RE, and their RE-TM indirect exchange coupling interaction. The high orbital moment of its unquenched  $4f$  orbital and the high energy of its spin-orbit coupling makes the RE act as a strong and localized magnetic moment whose orientation depends on the interatomic exchange and the crystal field at its particular local atomic environment. These two interactions are mainly provided by their TM neighbors whose RE-TM interaction energies overwhelm those of RE-RE. Since the RE-TM magnetic exchange

coupling is antiferromagnetic in spin, RE-TM alloys are ferrimagnetic for heavy REs like dysprosium. This interaction is usually treated as a molecular field whose intensity is calculated to be of the order of 200 T for crystalline DyCo<sub>5</sub> [13]. The energy of this interaction is, at least, one order of magnitude smaller than the TM-TM exchange. This range of values is comparable to  $k_B T$  energies, giving rise to different magnetic configurations as a function of temperature and RE concentration. A characteristic parameter that defines these ferrimagnetic alloys is their compensation temperature,  $T_{\text{comp}}$ , the temperature where the magnetic moment of the RE and TM sublattices cancel to each other.

Given the radical different magnetic behavior of the RE and the TM, the understanding of the magnetism of these alloys requires a precise characterization of the magnetic moment and anisotropy of the RE and TM sublattices separately. The perfect technique to do so is x-ray magnetic circular dichroism (XMCD) spectroscopy. The magnetic properties of the RE and TM sublattices can be studied separately by tuning the incident circularly polarized x rays to the corresponding absorption edges of the RE ( $M_{4,5}$ , probing its  $4f$  orbital) and the TM ( $L_{2,3}$ , probing its  $3d$  orbital) [14–16]. This is actually the technique of choice for the study of RE-TM alloys in the form of thin films because it allows *ex situ* sample preparation and it can be sensitive to regions at different depths of the sample by changing the way the x-ray absorption spectra is detected. Surface sensitivity is attained using total electron yield (TEY) detection, with probed depths of the order of

\*jidi@uniovi.es

2 to 3 nm, whereas fluorescence yield or x-ray transmission are more bulk-sensitive techniques. The simultaneous use of these two detection modes has been proven to be important for a correct understanding of these alloys. The different  $T_{\text{comp}}$  measured in these alloys using TEY and bulk detection [5], together with the reported RE segregation at their surface [17,18], has been used as an argument to explain interesting phenomena that occur at temperatures near their  $T_{\text{comp}}$  when the applied magnetic field is intense enough. The hysteresis loops of some DyCo alloys of similar concentration than the samples used in this study presented side wing loops at high applied fields as presented in some spring magnetlike bilayer structures [3,4,19]. The effect was explained as derived from the effective different RE concentrations at the bulk and the region near the surface, which will yield two different  $T_{\text{comp}}$  for each region [5,20].

In these studies, the  $T_{\text{comp}}$  at the region near the surface was estimated from the magnetic moments of cobalt and dysprosium deduced by XMCD measurements done using TEY detection. In all the cases, the analysis has always assumed the presence of a single dysprosium magnetic phase. However, due to the structural disorder of these alloys, different grades of intensity in the magnetic exchange interaction between dysprosium and cobalt are expected. Such effects should be stronger at the surface whose assumed larger RE concentration is driven by RE-RE bonding preference. Previous XMCD studies in NdCo alloys conducted by us using TEY detection [21] reported a substantial proportion of RE atoms that behaved as if they were paramagnetic, indicating that not all the RE atoms probed might have the same exchange interaction strength with the TM and, therefore, the same magnetic orientation distribution. Although those experiments were sensitive to the surface, their exact distribution was not demonstrated. Actually, Extended X-ray Absorption Fine Structure spectroscopy (EXAFS) experiments performed by us in similar samples deduced the possible presence of RE segregation in the bulk as well [22]. The possible existence of paramagnetic RE atoms nonexchange coupled to the TM due to disorder or/and RE segregated would contribute to overestimate the  $T_{\text{comp}}$  at the surface because its average magnetic moment orientation would be in the same direction of the applied field.

This effective bilayer interpretation of the side wing loops in DyCo films has been contested by others who consider that the observed effect is due to a spin flop phase transition [23]. The range of temperatures and fields under which this transition is produced can be predicted by the  $H - T$  (applied field  $H$  temperature) phase diagram of the alloy which is built by considering all the interactions present in the alloy. These studies show that the relative magnetic anisotropy of the RE and TM sublattices [23] and the interaction of the alloy at the interface with other metals [23] are key to understanding these spin-flop transitions.

It is clear, then, the importance of having a good characterization of the magnetism of these alloys at the region near the surface or at their interface with other materials whose magnetic structure could be complex. The purpose of the experiment presented in this paper is to improve the spectroscopical tools to understand the magnetic behavior of the TM and the RE sublattices, their mutual interaction, and their magnetic anisotropy using the information extracted from the

x-ray absorption spectra of the RE atoms, and consider their possible inhomogeneous distribution in depth at the region probed by TEY.

For this experiment, we prepared DyCo thin films anisotropically uniaxial with high perpendicular magnetic anisotropy (PMA) energies. Their anisotropy fields at 2 K,  $H_K$ , were well above the range of available field intensities in the experiment. Measurements were done at 2 K and RT. These two temperatures were distant enough from the  $T_{\text{comp}}$  of the alloys to avoid possible spin flip (and flop) effects. Also, it permitted us to measure in the regions where each of the sublattices were magnetically dominant (cobalt at RT and dysprosium at 2 K). At 2 K, thermal disorder was reduced to a minimum.

The ferrimagnetic character of DyCo alloys permits us to detect dysprosium atoms magnetically uncoupled from cobalt since they will be oriented in the opposite direction than their counterpart exchange-coupled dysprosium atoms at temperatures above  $T_{\text{comp}}$ , where the cobalt sublattice is magnetically dominant. Their detection requires a deconvolution of the RE  $M_{4,5}$  spectra in their parallel, antiparallel, and transverse components of  $J_z$  which are specially well defined in dysprosium. This deconvolution has been presented before in DyCo films [24] but it was not linked to the moment orientation of the dysprosium magnetic moments as done and explained in detail in this paper. Also, we use the XMCD spectra to deconvolve these components from the circularly polarized spectra instead of relying completely on their theoretically calculated shapes, as the mentioned work tried.

We show the potential of this technique in the study of the interaction between RE and cobalt atoms at the region probed by TEY by measuring at different orientation angles under a strong PMA. This technique is able to detect the presence of a RE segregated layer that affects in a significant way the measured moment of the RE. The presence of this layer seems intrinsic to the thin film growth in RE-TM alloys. Even removing the effect of this layer, the proportion of dysprosium atoms directly engaged in the PMA anisotropy of the alloy probed by TEY was not majority, possibly due to the extended thickness of the cobalt-depleted layer caused by the dysprosium segregation.

The paper is organized as follows: First, sample preparation and experimental details for XMCD data acquisition are described. Next, after showing the VSM magnetometry characterization of the measured films, the XMCD experimental results for each elemental sublattice are presented and discussed separately. This is followed by a section dedicated to explain how the deconvolution of the Dy  $M_5$  spectra is made, with the calculation details shown in an Appendix section. After this explanation, a model to fit the Dy  $M_5$  of the measured samples using the deconvolved spectral components is proposed, which consisted of two layers with different dysprosium moment distributions. The results of the fits are presented and discussed. The final section is the conclusion of the paper.

## II. EXPERIMENT

The two studied DyCo thin films were prepared at RT by magnetron sputtering at a base pressure of  $10^{-8}$  mbar

and  $10^{-3}$  mbar Ar pressure. They were grown onto silicon wafer substrates using two separate magnetron guns set at normal (cobalt gun) and at  $30^\circ$  angle incidence (dysprosium) with respect to the normal to the sample. Dysprosium and cobalt concentrations were calibrated using a quartz balance. The deposition method was different for each sample. A sample called DCC was prepared by codeposition of cobalt and dysprosium. A sample called DCM was grown by the alternate deposition of cobalt and dysprosium layers. The nominal thickness of the cobalt and dysprosium layers was 4.9 Å and 2.8 Å, respectively. The topmost deposited layer was cobalt. This second preparation method was intended as a way to estimate the importance of the interdiffusion between the elements forming the alloy in their structure and magnetic properties. All the samples were protected with a 20-Å-aluminum capping layer. The mean atomic concentration in the alloys was determined by electron-induced fluorescence spectroscopy. The difference in concentration between both films was relatively small. Sample DCC contained more dysprosium ( $\text{DyCo}_{4.4\pm 0.05}$ ) than the DCM film ( $\text{DyCo}_{4.6\pm 0.05}$ ). Their nominal thickness was 35 nm.

The structure of the alloys, deduced from x-ray diffraction measurements, was noncrystalline. Pure cobalt grain texture peaks disappeared at the RE concentrations of the analyzed samples, indicating the known amorphization effect of the RE on cobalt [25]. NdCo alloys studied by EXAFS, prepared in similar conditions and with the same concentrations of the analyzed samples, showed an extremely disordered atomic environment for the RE, whereas cobalt atoms seemed to cluster in grains of few atoms [22]. A similar structure is expected for the DyCo alloys due to the similar chemistry of Nd and Dy with cobalt.

X-ray circularly polarized absorption spectra were obtained at the HECTOR endstation [26] of the BOREAS BL-29 beamline at the ALBA synchrotron using TEY detection. HECTOR has a cryomagnet that can apply up to  $\pm 6$  T along the x-ray beam direction at different sample orientations, which in our case ranged from normal incidence ( $0^\circ$ ) to near grazing incidence ( $70^\circ$ ). The cryomagnet works at ultrahigh vacuum conditions (pressure within the  $10^{-10}$  mbar range). A liquid He cryostat permits fixing the sample temperature between 2 K and 350 K. Circularly polarized light was produced by an APPLE II elliptical undulator. Each XMCD spectra was the result of four spectra taken at opposite circular polarization helicities and magnetic field orientations.

### III. EXPERIMENTAL RESULTS AND DISCUSSION

#### A. Magnetometry

Both samples presented PMA even at RT. Figure 1 shows vibrating sample magnetometer (VSM) measurements of the variation with the temperature of the coercive field and the magnetization in remanence of samples DCC and DCM, together with their hysteresis loops obtained at 2 K. The values of the magnetization in remanence were obtained after magnetic saturation of the films with a field of 9 T at 5 K applied normal to their plane [27]. The remanent magnetization at 2 K was 75% and 83 % of the saturation magnetization in samples DCM and DCC, respectively. Table I summarizes these mag-

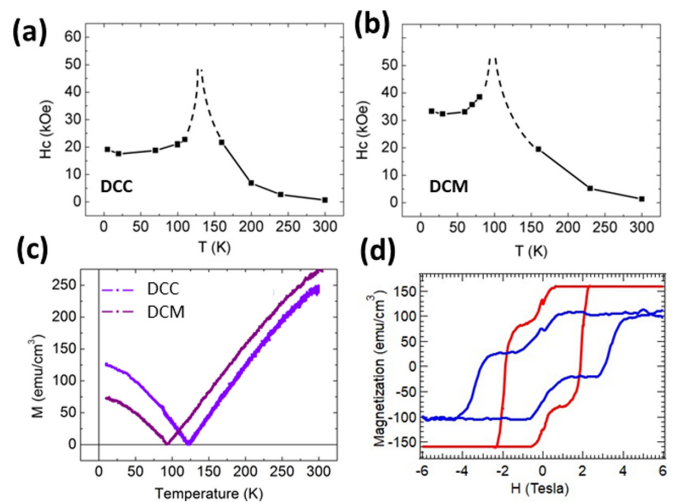


FIG. 1. Magnetic properties of samples DCC and DCM: (a), (b) are the variation in the coercive field as a function of the temperature of samples DCC and DCM, respectively, (c) is the magnetization in remanence as a function of the temperature for the two samples, (d) shows the hysteresis loop of samples DCC (red line, smaller coercive field) and DCM (blue line, bigger coercive field).

netic properties of the two samples at the two temperatures measured by XMCD (RT and 2 K) and their compensation temperatures,  $T_{\text{comp}}$ .  $T_{\text{comp}}$  was smaller in sample DCM (90 K) than in sample DCC (125 K). These values agree with their different RE concentrations, and with that expected by comparing with the reporting by others in DyCo alloys of similar concentrations [5,20], assuming a linear relationship between  $T_{\text{comp}}$  and the atomic concentration of the alloy [18]. The higher cobalt concentration in sample DCM causes a marked lower magnetic remanence at 10 K than in sample DCC. This explains the large difference between the coercive fields measured at 10 K, higher in sample DCM (3.5 T) than in sample DCC (1.9 T). However, sample DCM has a higher  $H_C$  at RT, when its  $M_S$  is higher. X-ray reflectometry shows rougher surfaces in DCM than in DCC thin films, suggesting that the larger  $H_C$  of the DCM thin film is probably caused by its higher density of domain-wall pinning defects. The response to the magnetic field of the analyzed samples differed from those reported in DyCo thin films of similar concentration [5,20]. The coercive fields of both samples were notoriously higher and the loops were not squared at temperatures below RT, indicating that their internal structure, which is responsible for the way cobalt and dysprosium sublattices magnetically interact, was somehow different.

TABLE I. Compensation temperature,  $T_{\text{comp}}$ , Magnetic remanence,  $M_R$ , and coercive field,  $H_C$ , of samples DCC and DCM at 2 K and RT [27].

Sample	$T_{\text{comp}}$	Temperature	$M_R$ (emu/cm <sup>3</sup> )	$H_C$ (T)
DCC	125 K	2 K	125	1.9
		300 K	250	0.2
DCM	90 K	2 K	75	3.5
		300 K	275	0.4

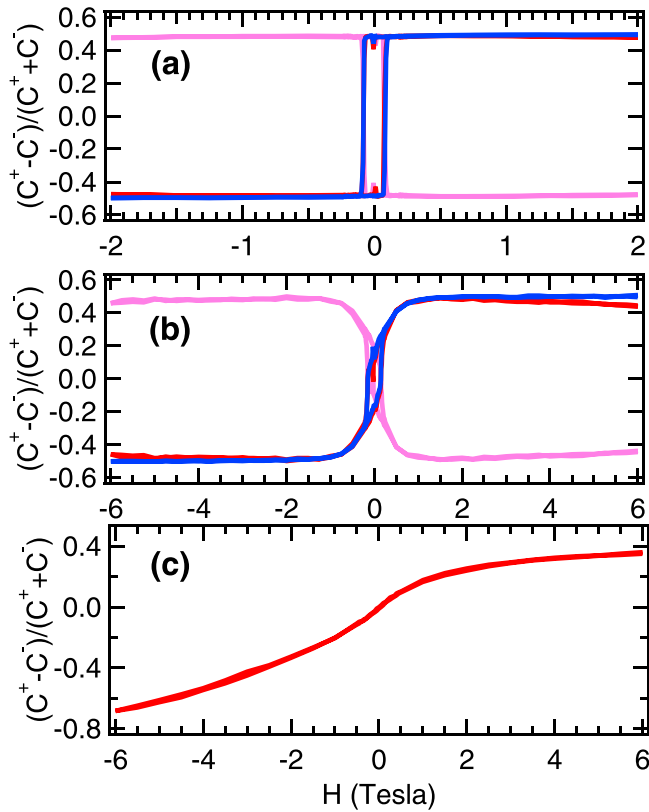


FIG. 2. Hysteresis loops taken at the Dy  $M_5$  (pink) and Co  $L_3$  (blue) edges at RT: (a) normal orientation, (b) grazing incidence ( $70^\circ$ ). The hysteresis loop of the dysprosium sublattice multiplied by  $-1$  has been drawn in red behind the cobalt loop for comparison. (c) Dysprosium hysteresis loop taken at 2 K at grazing incidence ( $70^\circ$ ).

The shape of the hysteresis loops measured by VSM along the perpendicular axis of the sample rapidly evolved with decreasing temperature from square loops at RT to wasp-waist shaped loops, as shown in Fig. 1, starting at 240 K. There are different ways to obtain this kind of loop [28]. Most of them require an AF interaction between magnetic phases with contrasting coercivities or anisotropies [29], indicating a possible nonuniform distribution of cobalt and dysprosium in the films. As will be shown, such a structure agrees with the results obtained from the analysis of their TEY spectra. This might explain the relatively large coercive fields of the analyzed samples and the absence of triple hysteresis loops at fields below 6 T at temperatures close to their  $T_{\text{comp}}$ , as reported in samples of similar concentration and thickness [5,20].

### B. XMCD hysteresis loops

Figure 2 shows the hysteresis loops of sample DCC at RT and 2 K for the cobalt and dysprosium sublattices obtained by measuring the intensity of the Co  $L_3$  peak and the Dy  $M_5$  peak, respectively. Their change in shape with field orientation at RT [Figs. 2(a) and 2(b)], from squared at  $0^\circ$  orientation to S shaped at  $70^\circ$  field orientation, shows that the samples had PMA, as observed by VSM magnetometry. The loops of the cobalt and dysprosium sublattices are nearly

identical. A small decoupling between both sublattices is only noticeable at high fields. The magnetization of cobalt remains constant at high fields up to 6 T whereas that of dysprosium seems to decrease steadily with the increasing field from zero field.

A similar kind of decoupling, although more pronounced than in the present case, has been observed in NdCo films [21]. The effect was caused by a portion of Nd that was paramagnetic. In the present case, the reduction in the dysprosium magnetization must come from dysprosium atoms which must be AF oriented at the saturation field. This should be paramagnetic dysprosium, but also dysprosium which is poorly AF coupled to cobalt.

At 2 K, only the hysteresis loop of the dysprosium sublattice in sample DCM was taken at near the plane field orientation ( $70^\circ$ ), shown in Fig. 2(c). The shape of the loop shows that the films were far from being magnetically saturated up to 6 T, indicating that the PMA energy of the samples was strongly increased at this temperature. The lack of a coercive field in the loop shows that the measured magnetic moments experienced a progressive rotation with the applied field intensity. The loop shows a shape asymmetry between the positive and negative branches.

### C. XMCD Cobalt

The magnetic moments of cobalt were deduced from their  $L_{2,3}$  spectra. The method used to extract the cobalt absorption coefficient to correctly apply the XMCD sum rules [30,31] is fully described in Ref. [21] and it considers saturation effects [32]. The number of holes was calculated comparing their unpolarized absorption spectra with that of a pure cobalt reference sample deposited in similar conditions as the rest of the films. The number of holes for this reference sample was set to the tabulated for pure cobalt, 2.49, yielding a magnetic moment at 2 K of  $1.79 \pm 0.02 \mu_B$ , which is similar to that measured by others ( $1.77 \mu_B$ ) [33]. As can be observed from Figs. 3(a) and 3(b), the shape of the spectra was almost identical to the cobalt reference except in their intensity, which was lower and almost independent of the sample orientation angle or temperature. Their number of holes reduced to approximately 91% those of pure cobalt. The total magnetic moment of the samples together with the related orbital and spin components and orbital to spin ratios are shown in Table II. The total magnetic moment of the two alloys at 2 K and normal incidence (easy magnetic axis) was similar within the error, of the order of  $1.33 \pm 0.03 \mu_B$ . This value is in agreement with that expected from those observed in NdCo alloys as a function of the number of holes [21], and they would correspond to a RE concentration higher than the nominal, of the order of DyCo<sub>3.5</sub>. The magnetic moment obtained at RT (only measured at normal incidence in DCC) was practically the same than at 2 K,  $1.34 \pm 0.03 \mu_B$ .

The anisotropy of the orbital moment and the dipolar moment [14,34] were  $\Delta m_L = m_{0^\circ} - m_{70^\circ} = -0.04$  and  $-0.013 \mu_B$ , respectively. These values are small. They discard cobalt as the source of PMA in the films. The negative sign indicates an in-plane anisotropy for the cobalt sublattice at RT [14,35,36]. This is in coincidence with what we observed in NdCo alloys [21] and it is the expected behavior if dysprosium

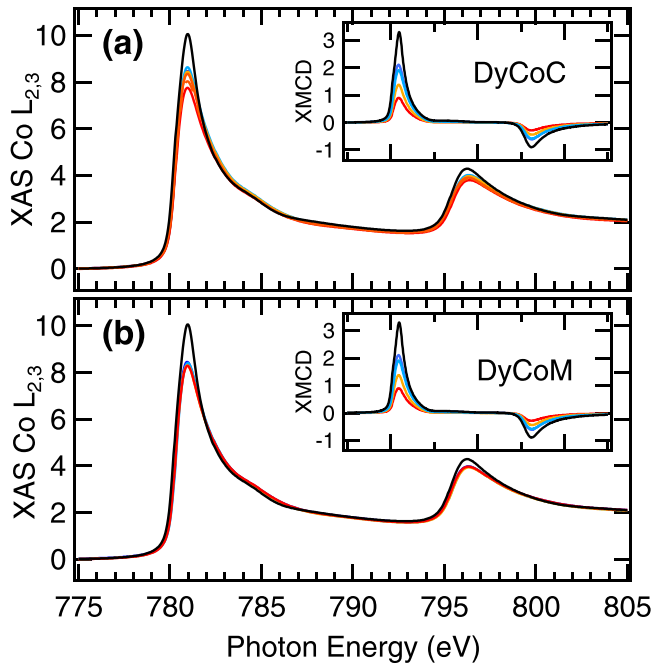


FIG. 3. X-ray absorption (XAS) spectra obtained at the Co  $L_{2,3}$  edge of a pure cobalt thin film compared with the spectra of cobalt in (a) DCC and (b) DCM thin films taken at 2K and 0° (blue), 20° (green), 45° (orange), and 70° (red) beam incidence angles (magnetic field orientation angle) with respect to the normal to the sample. The most intense spectrum (black line) is from pure cobalt. In the inset, the XMCD spectra taken at different orientation field angles, using the same code color.

causes the observed PMA of the samples because of the oblate shape of its  $4f$  orbital.

The total magnetic moment measured at 2 K is displayed in Fig. 4 as a function of the field orientation angle. It decreases in both samples with increasing field angle orientations because of the uncompleted magnetic saturation of the alloy at the 6 T applied field. The dashed curve displayed in Fig. 4 is the fit of the averaged magnetic moments of the two samples using a cosine function plus a constant. The constant could be interpreted as the portion of the cobalt magnetic moment that it is oriented parallel to the field. This constant is only 10% of the total intensity, indicating that most of the cobalt magnetic moments were fixed at the easy axis direction.

The orbital magnetic moment at 0° field orientation increased a small quantity in both samples with respect to their value at RT, from  $0.12 \mu_B$  to  $0.16 \mu_B$  (sample DCC). For the rest of the field-orientation angles, only the orbital to effective spin moments ratio can be compared because of the uncompleted magnetic moment saturation of the films. This ratio is the highest at 0° and it decreases in both samples, from 0.14 at normal orientation to 0.09 (0.10 at 70° in sample DCC). This decrement was small but the effect appeared in both samples. It might indicate that the PMA of the alloy involves either an anisotropy in the orbital moment of cobalt in the same direction of the easy axis or a larger effective spin component at angles far from the easy axis, which might come from cobalt atoms in more isotropic locations.

TABLE II. Total magnetic moment ( $m_{\text{tot}}$ ), effective spin ( $m_s^*$ ) moment, orbital ( $m_o$ ) moment, and its ratio  $m_o/m_s^*$ , of cobalt obtained by XMCD in DyCo alloys (samples DCC and DCM) and YCo alloys (YCC and YCM). All moments are given in  $\mu_B$  units.  $m_s^*$  and, therefore,  $m_{\text{tot}}$  have not been corrected by the  $m_{T_z}$  term, the dipole moment of spin. Error bars are of the order of 2% for  $m_s$  and  $m_o$ . As a reference, pure cobalt (thin film) at 2 K:  $m_s = 1.58 \mu_B$ ;  $m_o = 0.21 \mu_B$ ;  $m_{\text{tot}} = 1.79 \mu_B$

Sample	T		Field orientation angle			
			0°	20°	45°	70°
DCC	RT	$m_s^*$	1.22	—	—	1.11
		$m_o$	0.12	—	—	0.16
		$m_{\text{tot}}$	1.34	—	—	1.25
		$m_o/m_s^*$	0.09	—	—	0.12
	2 K	$m_s^*$	1.17	1.15	0.91	0.41
		$m_o$	0.16	0.10	0.08	0.06
		$m_{\text{tot}}$	1.33	1.25	0.99	0.50
		$m_o/m_s^*$	0.14	0.09	0.09	0.10
DCM	RT	$m_s^*$	—	—	—	1.08
		$m_o$	—	—	—	0.16
		$m_{\text{tot}}$	—	—	—	1.24
		$m_o/m_s^*$	—	—	—	0.15
	2 K	$m_s^*$	1.15	1.10	0.79	0.54
		$m_o$	0.15	0.10	0.06	0.04
		$m_{\text{tot}}$	1.30	1.20	0.85	0.58
		$m_o/m_s^*$	0.13	0.09	0.08	0.09
YCC	2 K	$m_s^*$	1.28	—	1.24	1.28
		$m_o$	0.14	—	0.19	0.16
		$m_{\text{tot}}$	1.42	—	1.43	1.44
		$m_o/m_s^*$	0.11	—	0.16	0.13
YCM	2 K	$m_s^*$	1.26	—	1.18	1.22
		$m_o$	0.07	—	0.18	0.17
		$m_{\text{tot}}$	1.33	—	1.36	1.39
		$m_o/m_s^*$	0.06	—	0.15	0.14

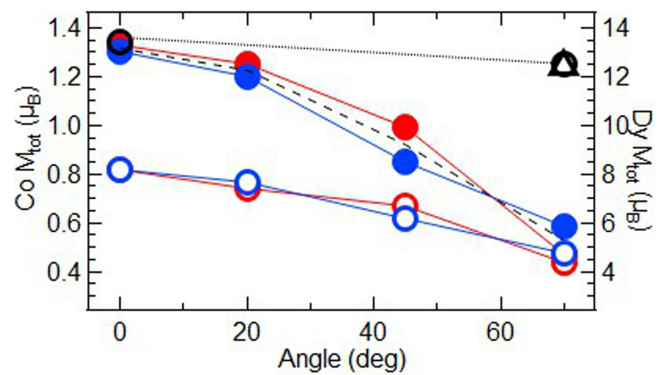


FIG. 4. Total magnetic moment of cobalt (solid dots) and dysprosium (empty dots) in samples DCC (red dots) and DCM (blue dots) measured at 2 K. The black dashed line in (a) is the fit to a cosine function plus a constant. Black dots and triangles are cobalt moments measured at RT. The estimated error of the measurement is the width of the dots.

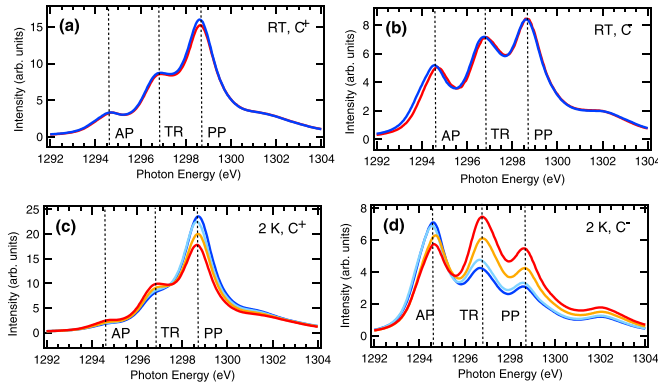


FIG. 5. Dy  $M_5$  spectra of sample DCM obtained at RT [spectra at (a), (b)] and 2 K [spectra (c), (d)]. The spectra taken with right-circular polarization are (a), (c). (b), (d) are the spectra taken using left-circular polarization. RT spectra were taken at  $0^\circ$  (dark blue line) and  $70^\circ$  (red line) incident angles. 2 K spectra were taken at  $0^\circ$  (dark blue line),  $20^\circ$  (light blue line),  $45^\circ$  (orange line), and  $70^\circ$  (red line) incident angles.

To discard that the observed anisotropy of the cobalt magnetic moment was only caused by the chemical bonding to the RE, YCo films deposited in similar conditions of concentration, film thickness and deposition process were measured by XMCD. The chemical interaction of yttrium is equivalent to that of RE, with a nearly empty  $4d$  band but without an occupied  $4f$  orbital, i.e., with no  $4f$  magnetic moment. Actually, the YCo phase diagram is very similar to that of DyCo [37,38]. Therefore, the atomic structure of the YCo alloy should be similar to that of DyCo. The magnetic moments of cobalt in YCo measured at RT (normal orientation only) and 2 K are displayed in Table II. The values are about 10% smaller in the multilayer than in the continuous film and they increase in both films when temperature goes from RT to 2 K, in contrast to the observed in the DyCo alloys where there was almost no difference. The YCo alloys were magnetically soft and their magnetic anisotropy was in the plane. Their orbital to effective spin ratios were similar to that found at normal orientation in the DyCo films but they did not show the strong decrease in their value with the increasing orientation angle as observed in DyCo. This fact, together with the cosinelike variation in the total magnetic moment of cobalt in the DyCo films, indicates that their probed cobalt atoms are mostly located at magnetically anisotropic environments. By comparison with the YCo alloy, the magnetic anisotropy found in the cobalt sublattice of the DyCo films must be induced by the magnetic interaction with the dysprosium atoms. Therefore, a similar angle variation in the magnetic moment of the dysprosium sublattice as that found in cobalt would be expected.

#### D. XMCD Dy

In dysprosium, the most relevant changes in the spectra occur in the Dy  $M_5$  edge. Figure 5 shows the Dy  $M_5$  taken in sample DCM at RT and 2 K for the two circular polarizations at different angles. Sample DCC showed similar changes. The Dy  $M_5$  spectral shape is defined by three intense

TABLE III. Effective spin moment,  $m_s^*$ , orbital moment,  $m_o$ , dipole moment of spin,  $m_{T_z}$ , and total magnetic moment,  $m_{\text{tot}}$ , of dysprosium obtained by XMCD in samples DCC and DCM. All moments are given in  $\mu_B$  units. The estimated error bars is of 2% in  $m_s^*$ ,  $m_o$ , and  $m_{T_z}$ .  $m_{T_z} = \frac{m_o}{6} [\frac{m_s^*}{m_o} - \frac{m_s}{m_o}]$  [15], using the theoretical value of  $\frac{m_s}{m_o} = 0.475$  [16].  $m_{\text{tot}} = m_o + (m_s^* - 6m_{T_z})$ .

Sample	T		Field orientation angle			
			$0^\circ$	$20^\circ$	$45^\circ$	$70^\circ$
DCC	RT	$m_s^*$	-1.92	—	—	-1.92
		$m_o$	-1.42	—	—	-1.41
		$m_{T_z}$	-0.09	—	—	-0.10
	$m_{\text{tot}}$	-2.78	—	—	-2.74	
	2 K	$m_s^*$	2.78	2.51	2.19	1.46
		$m_o$	4.19	3.81	3.42	2.23
$m_{T_z}$		0.26	0.23	0.19	0.13	
$m_{\text{tot}}$	8.18	7.43	6.67	4.35		
DCM	RT	$m_s^*$	—	—	—	-0.91
		$m_o$	—	—	—	-1.44
		$m_{T_z}$	—	—	—	-0.07
	$m_{\text{tot}}$	—	—	—	-2.81	
	2 K	$m_s^*$	2.84	2.64	2.14	1.61
		$m_o$	4.21	3.93	3.17	1.61
$m_{T_z}$		0.28	0.26	0.21	0.15	
$m_{\text{tot}}$	8.2	7.66	6.19	4.73		

peaks, marked in the figure as peaks AP, TR, and PP, which are located at photon energies 1294.5 eV, 1296.7 eV, and 1298.6 eV, respectively. Their relative intensity changes with the polarization sign and with the field orientation angle. At RT, the changes with the angle are small, but they are very evident at 2 K. At this temperature, peak PP is the most intense at  $C^+$  polarization and normal incidence. Within the same polarization, peak PP decreases in intensity as the field orientation angle (incident x-ray beam angle) increases. The opposite is observed using  $C^-$  polarization. In this case, the peak marked AP is the most intense at normal incidence. For both polarizations, peak TR increases in intensity when the incident angle increases. As will be shown, peaks PP, AP and TR are associated to electronic transitions to states where the magnetic moment of the related  $4f$  orbital is parallel, antiparallel, or transverse to the circularly polarized x-ray beam wave vector, respectively. It is important to note that, at RT, peak PP is also the most intense in  $C^-$  polarization. This is opposite to what happens at 2 K, especially at  $70^\circ$ , where the measured magnetic moment of dysprosium is the lowest and comparable to that measured at RT.

The XMCD spectra of the Dy  $M_{4,5}$  edge were analyzed following the process explained in Ref. [21]. Table III shows the magnetic moments of dysprosium in each of the samples at RT and 2 K. The relative weakness of the AF interaction with cobalt and the structural disorder of the alloy makes the magnetic moment of the dysprosium atoms be dispersed in its orientation with respect to the cobalt magnetic moment, forming what is called an asperomagnet [39]. The moment orientation of the RE atoms when the alloy is magnetized in the easy axis is usually taken as uniform and symmetrically distributed around this axis within a cone with a half opening

angle  $\theta_C$  (for instance,  $\theta_C = \pi/2$  represents the distribution of moments in a semisphere). For field orientations away from the easy axis, a dispersion in the shape and opening angle of the cone is expected. In this case, we assume that the resulting distribution of the dysprosium can be approximated by a cone that has its symmetry axis deviated from the field direction, an angle  $\varphi_C$ . The magnetic moment measured is the averaged sum within the cone of the magnetic moment component along the field orientation axis. At the easy axis, this sum is  $M_{Dy} \cos^2 \theta_C/2$ , where  $M_{Dy}$  is  $9.8 \mu_B$ , the dysprosium magnetic moment of its  $4f$  orbital. The magnetic anisotropy would then change the value of the measured magnetic moment by opening the cone angle and changing its symmetry axis orientation.

At RT, the dysprosium magnetic moment has almost no difference at both orientations, as expected from the hysteresis loops. The PMA of dysprosium doesn't have enough energy to distort its magnetic moment distribution cone at RT. There is not a significant variation between the values obtained in both samples, which are about  $-2.8 \mu_B$  (sample DCM only measured at  $70^\circ$  field orientation). This quantity is small. The lowest magnetic moment that can be measured assuming that all dysprosium atoms are AF coupled to Co, i.e., uniformly distributed within a cone of half opening angle  $\theta_C = \pi/2$  (semisphere), is  $M_{Dy}/2 = -4.9 \mu_B$ , i.e., half the value of its total magnetic moment. This means that there should be dysprosium atoms with their moment orientation opposite to that of those AF coupled to cobalt. Theoretical calculations estimated that the averaged magnetic moment of Dy decays to half its value at about 300 K in crystalline DyCo<sub>5</sub> [40]. The lower values observed in the present case should have to do with the intrinsic disorder of the measured alloys, with dysprosium atoms distributed in different atomic environments where, in some of them, the exchange coupling to cobalt should be weaker than in crystalline DyCo<sub>5</sub> or possibly nonexistent. The analysis of the Dy  $M_5$  spectra exposed in a later section searches to understand how these dysprosium atoms are distributed through the depth proved by TEY and how this can affect the TEY measurements, including the possible presence of segregated dysprosium at the interface with the aluminum capping layer.

Figure 4 (right-side scale) displays the variation of the dysprosium magnetic moment as a function of the field orientation angle at 2 K compared to that of cobalt. Both samples have similar values which decay with the angle at a slower pace than in the cobalt sublattice. This magnetically less anisotropic behavior of dysprosium is somehow contrary to what was expected: the magnetic moment of the RE should be, compared to cobalt, the one fixed with the highest energy to the easy axis since the PMA in these alloys must stem from it, as deduced from the analysis done in the previous section (Sec. III C). The total magnetic anisotropy of the alloy should depend on the distribution of the crystal field orientation at the RE sites [2] and its influence on the magnetic moment of the bonding TMs at each RE site. Following the single ion anisotropy model [2], both crystal field and RE-TM indirect exchange are expected to be tightly related. Therefore, the RE environments that most contribute to the magnetic anisotropy of the alloys should be strongly exchange coupled to the TM as well.

The magnetically less anisotropic character of the measured dysprosium sublattice indicates that only a portion of the dysprosium atoms probed by TEY should be active magnetic anisotropy generators. The magnetic field felt by dysprosium is the sum of the external applied field and the molecular field, which is mainly provided by the interatomic exchange interaction with cobalt atoms, whose strength can be estimated in, at least, more than 150 T [21]. As has been observed, the rotation of the cobalt moment at grazing orientations is small. Therefore, the effective molecular field felt by the dysprosium should be closer to that of the applied field at those sample orientation angles, meaning that a portion of the probed dysprosium should be somehow decoupled or poorly coupled to cobalt, as stemming from the analysis done at RT. One of the challenges in the analysis of the Dy  $M_5$  spectra, shown in the next sections, is to determine the location of the dysprosium which are apparently weakly interacting to cobalt.

A way to compare the magnetization measured in the bulk with the magnetization measured near the surface (XMCD using TEY) is to evaluate how these magnetic moments found by XMCD fit with those deduced from VSM, shown in Table I. When the magnetic moment of the cobalt used to calculate the total magnetization of the alloy is that obtained by XMCD,  $1.33 \mu_B$ , the magnetic moment of dysprosium that it is needed to match the magnetization measured by VSM at RT is  $3.8 \mu_B$ ,  $1 \mu_B$  above that measured by XMCD. This value is still below the expected if all dysprosium magnetic moments were AF coupled to cobalt. When the same estimation is done at 2 K, the magnetic moment expected for dysprosium is  $7.3 \mu_B$ , close to  $1 \mu_B$  smaller than that found by XMCD. These differences between bulk (VSM) and surface (XMCD) are similar to the reported by Chen *et al.* [5] and Luo *et al.* [20]. The explanation given to this effect in those cited reports was the presence of a higher dysprosium concentration at the region near surface than in the bulk due to RE segregation in their samples. If that was happening in our samples, their cobalt and dysprosium moments in the bulk should be higher than that measured by XMCD. For instance, if the cobalt moment in the bulk raised to  $1.50 \mu_B$ , the related dysprosium moment should be  $4.7 \mu_B$ , which is almost  $2 \mu_B$  higher than that measured by XMCD. This would set the surface at a higher  $T_{\text{comp}}$  than in the bulk.

The  $T_{\text{comp}}$  of a ferrimagnetic RE-TM alloy essentially depends on the magnetic exchange strength between the RE and the TM atoms. If the segregated RE atoms at the region near the surface do not bond tight to cobalt, their exchange interaction will weaken. The effect, in terms of magnetic moments, will be similar to an increase of the  $T_{\text{comp}}$  because, above this temperature, there will be dysprosium moments that will not be AF coupled to cobalt, reducing the total moment of the dysprosium sublattice. Below  $T_{\text{comp}}$ , the effect will be the opposite, i.e., they will add up in moment to the moment of the AF coupled-to-cobalt dysprosium. This is not an unlikely situation regarding the magnetic moments of dysprosium measured by XMCD, which are well below the expected if all RE atoms were AF coupled to cobalt. Moreover, if RE segregation occurs it is because it favors RE-RE metallic bonding. To demonstrate the presence of these two kinds of RE atoms requires a technique able to detect them.

The next section shows a way to do it in a quantitative way by analyzing the circularly polarized Dy  $M_5$  spectra. Dysprosium is especially well adapted for this kind of analysis, although it should be applicable to most REs, with the exception of those with  $L = 0$  like  $Gd^{+3}$ .

#### IV. SPECTRAL ANALYSIS METHOD FOR THE DY $M_{4,5}$ SPECTRA

##### A. Decomposition of the Dy $M_{4,5}$ spectrum

Like most REs, the electrons in the  $4f$  orbital of dysprosium are well screened by the valence band orbitals and they behave as in an isolated atom. Actually, the Dy  $M_{4,5}$  edge spectrum, which involves electronic transitions from the  $3d$  to the  $4f$  orbital, is practically insensitive to the dysprosium chemical environment and is well fitted by calculating it using only intratomic interactions [41,42]. The intensity of these transitions can be notably influenced by the bonding with other magnetic atoms through its indirect exchange magnetic interaction and the resulting crystal field. The relative weakness of these interactions permits us to treat them as perturbations whose most important effect is to break the degeneracy of the quantum number  $M$  of the  $4f$  angular momentum component  $J_z$ . When the interaction is magnetic, this effect consists of orienting the magnetic moment of the  $4f$  orbital along a specific direction.

Therefore, to a good approximation, only the intensity, but not the shape, of the Dy  $M_{4,5}$  lines are modulated by the orientation of the total angular momentum of the  $4f$  orbital with respect to the direction of the polarized x ray. The allowed transitions in the dipole approximation are those in which  $\Delta J = 0, \pm 1$ . If light is circularly polarized, only  $\Delta m = \pm 1$  transitions are allowed. Therefore, if the beam is perfectly oriented parallel (antiparallel) to the magnetic moment of the  $4f$  orbital, the resulting  $M_{4,5}$  spectrum will be built with only those excitations where  $\Delta J = 0, \pm 1$  and  $\Delta m = 1(-1)$ . We will call these spectral components PP if  $\Delta m = -1$  and AP when  $\Delta m = 1$ . The circular dichroism spectrum, XMCD, is the difference between these two spectrum. The sum rules related to these transitions give rise to the XMCD sum rules that permit determining both the magnetic spin and orbital moments of the  $4f$  orbital.  $\Delta m = 0$  transitions occur when the light is linearly polarized along the magnetic moment direction. This spectral component is not present in the XMCD spectrum because it depends on  $\langle M^2 \rangle$  [42]. We will call this component TR.

The excitations of all three spectral components PP, AP, and TR occur when the  $4f$  magnetic moment and the incident circularly polarized light are not parallel. This is because the electric field felt by the  $4f$  electrons is equivalent to the sum of two circularly polarized fields with opposite helicities, and a linear polarized field aligned in the direction of the magnetic moment. The detailed calculation of the amplitude of these fields is explained in Appendix. The dependency of the amplitude of these polarized field with the magnetic moment orientation angle  $\theta$  is

$$P = \frac{e^{\pm i\varphi}}{\sqrt{2}} \left[ \frac{(\cos \theta \pm 1)}{\sqrt{2}} P_{z_m}^{-1} + \frac{(\cos \theta \mp 1)}{\sqrt{2}} P_{z_m}^1 + P_{z_m}^0 \sin \theta \right]. \quad (1)$$

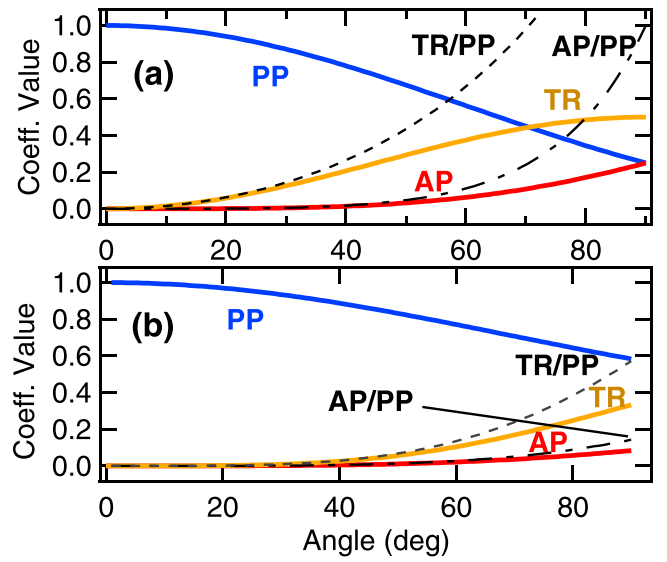


FIG. 6. Angle coefficients for PP, AP and TR as a function of (a) magnetic moment orientation angle with respect to the circularly polarized incident beam,  $\theta$ , and (b) cone half opening angle  $\theta_c$ .

$P_{z_m}^{-1}$ ,  $P_{z_m}^1$ , and  $P_{z_m}^0$  are the dipole operators for right- and left-circular polarizations, and linear polarization along the  $z$  axis, respectively.  $\varphi$  is an arbitrary phase. Taking into account the previous expressions, the modulation of the intensity of each of the spectral components (PP, AP, and TR) with the orientation angle  $\theta$  is given by the following expression (see Appendix):

$$\begin{aligned} &PP + AP + TR \\ &= \left[ \frac{(\cos \theta \pm 1)^2}{4} A_{JJ'}^{-1} + \frac{(\cos \theta \mp 1)^2}{4} A_{JJ'}^1 + \frac{\sin^2 \theta}{2} A_{JJ'}^0 \right], \end{aligned} \quad (2)$$

where  $A_{JJ'}^q$  are the reduced angular integers. They are directly related to the transitions  $\Delta J = 0, \pm 1$  and  $q = \Delta m$ . The distribution in energy and intensity of these transitions is well tabulated, both theoretically and experimentally [41–43]. Figure 6(a) displays the coefficients that multiply to the angular integers  $A_{JJ'}^q$ , shown in Eq. (2) as a function of the magnetic moment orientation angle  $\theta$  with respect to the incident beam. As expected, the coefficients that multiply to the TR ( $A_{JJ'}^0$ ) and AP ( $A_{JJ'}^1$ ) components increase their value only at angles closer to  $\pi/2$ .

The most common situation found in the studied alloys, which have no defined crystal structure, is the one in which the orientation of the magnetic moment of dysprosium is not well defined but is distributed over a range of angles due to structural and thermal disorder. This distribution is assumed to be uniform and symmetrical with respect to the axis of a cone with a half opening angle  $\theta_c$ . This distribution modifies the coefficients of the angular integers. The new coefficients in this situation are obtained by averaging the angle coefficients defined in Eq. (2) for each component within the cone angle  $\theta_c$ , resulting in the following expression as a function



of  $\theta_C$ :

$$\begin{aligned} \text{PP} + \text{AP} + \text{TR} = & \frac{1}{3} \frac{(1 - \cos^6 \frac{\theta_C}{2})}{\sin^2 \frac{\theta_C}{2}} A_{JJ'}^{-1} + \frac{1}{3} \sin^4 \frac{\theta_C}{2} A_{JJ'}^1 \\ & + \frac{1}{3} \frac{(\cos^3 \theta_C - 3 \cos \theta_C + 2)}{1 - \cos \theta_C} A_{JJ'}^0. \end{aligned} \quad (3)$$

Figure 6(b) shows the coefficients of each excitation component as a function of the cone half-opening angle  $\theta_C$ . The coefficients of the TR and AP components increment its value at large angles, but not as fast as in the case of a defined angle orientation. This is better observed when the ratio between the TR and AP components, shown in both figures, are compared. These ratios are substantially smaller in the cone angle coefficients [Fig. 6(b)].

When the cone has an inclination angle  $\varphi_C$  with respect to the beam direction, the components PP', AP', and TR' of the magnetic moment in the cone are projected in the beam axis following expression Eq. (2), substituting the angle  $\theta$  by  $\varphi_C$ . The PP' component is calculated using Eq. (3), the AP' component is the same as Eq. (2) but interchanging the factors  $A_{JJ'}^{-1}$  by  $A_{JJ'}^1$ , and the TR' component is calculated by multiplying TR by  $\sin^2 \theta_C/2$ .

Since the cross-section values of the angular integers are tabulated [41,42] and the angle dependent modulation of the PP, AP and TR components are known [Eqs. (2) and (3)], it is possible to determine the orientation of the magnetic moment of any RE in any chemical environment just by identifying their PP, AP, and TR components and checking their relative intensities. This is something that can be inferred also by comparing the magnetic moment deduced from the application of the XMCD sum rules and comparing it with the total magnetic moment of the RE. But this is only valid if there is a single magnetic form of dysprosium. Things become more complicated if the analyzed material contains RE in different magnetic states, i.e., RE with different magnetic moment orientation distributions. The deconvolution of the spectra in their PP, AP, and TR components is then required. This could be done by their direct calculation using numerical methods as the employed by Thole *et al.* [41]. This is the approach used in Ref. [24], but it is important to note that the build of the RE  $M_{4,5}$  spectrum only requires, to a good approximation, the shape of the spectral component, which can be isolated by spectral methods. The Dy  $M_5$  spectrum is especially suited for this kind of analysis.

Due to the large value of the orbital moment,  $L$ , of the  $4f$  orbital in dysprosium, the splitting between the PP and AP components in the  $M_5$  edge is the largest among the RE. Dy is the RE that has the lowest overlap between these two sets of excitations, which is estimated in less than 5% [42]. This eases the extraction of both spectral components from any XMCD spectra at the Dy  $M_5$  edge. Figure 7 shows the XMCD spectrum for Dy  $M_5$ . Only the PP and AP components are in the spectra, which are well distinguished because they have opposite signs. These two spectral shapes can be taken, as a first approximation, to the PP and AP true components of the spectra. The TR spectral component is extracted by subtraction of these two approximated components to the related circularly polarized spectra. For the subtraction, each

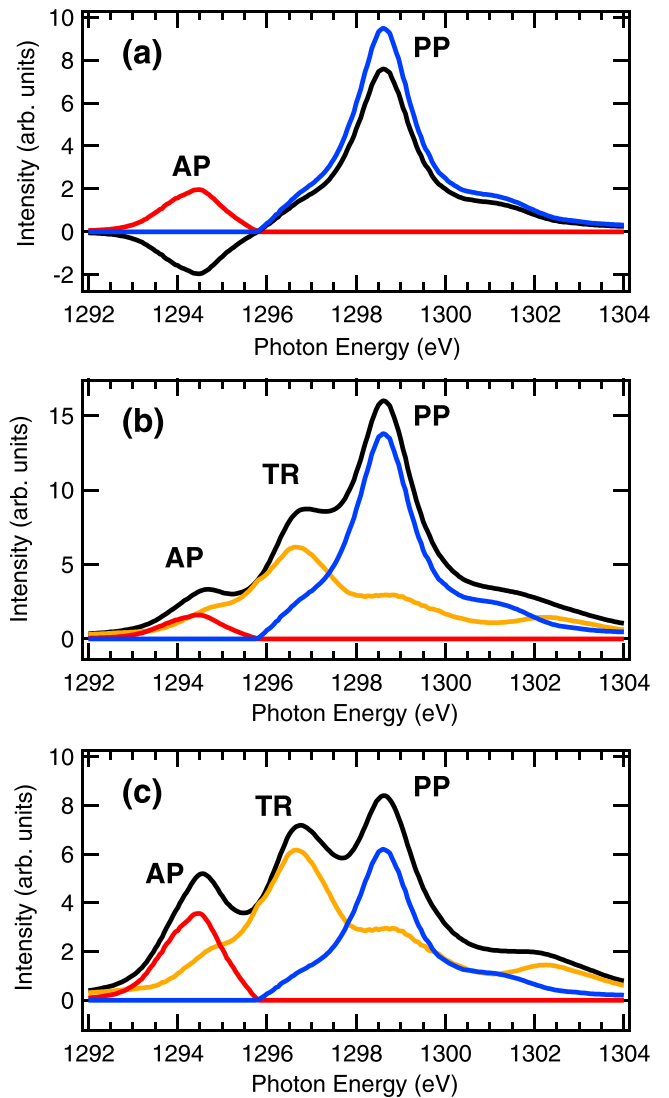


FIG. 7. (a) XMCD spectrum of the DCC sample at RT and normal incidence and its related PP and AP components; (b)  $C^-$  polarized spectrum of DCC sample taken at RT and normal incidence with their related PP, AP, and TR components; (c)  $C^+$  polarized spectrum of DCC sample taken at RT and normal incidence with their related PP, AP, and TR components

of the components must be multiplied by a coefficient which is related to its relative spectral intensity, which depends on the sum of all the RE magnetic moment orientation distributions probed. These coefficients must be the same in both circularly polarized spectra, bearing in mind that the PP and AP components are interchanged in the two polarizations when the spectra are taken at the same magnetic field direction. The determination of the value of these coefficients is not precise, since it depends on how well the shape of the TR component is known. In our approach, we used the spectral line shape theoretically calculated by Thole *et al.* [41]. This so-extracted TR component contains the overlap region between the PP and AP components. This produces some shape differences between the TR obtained at different beam orientation angles because the proportion of the TR component respect to the PP and AP components changes. In our case, the spectra

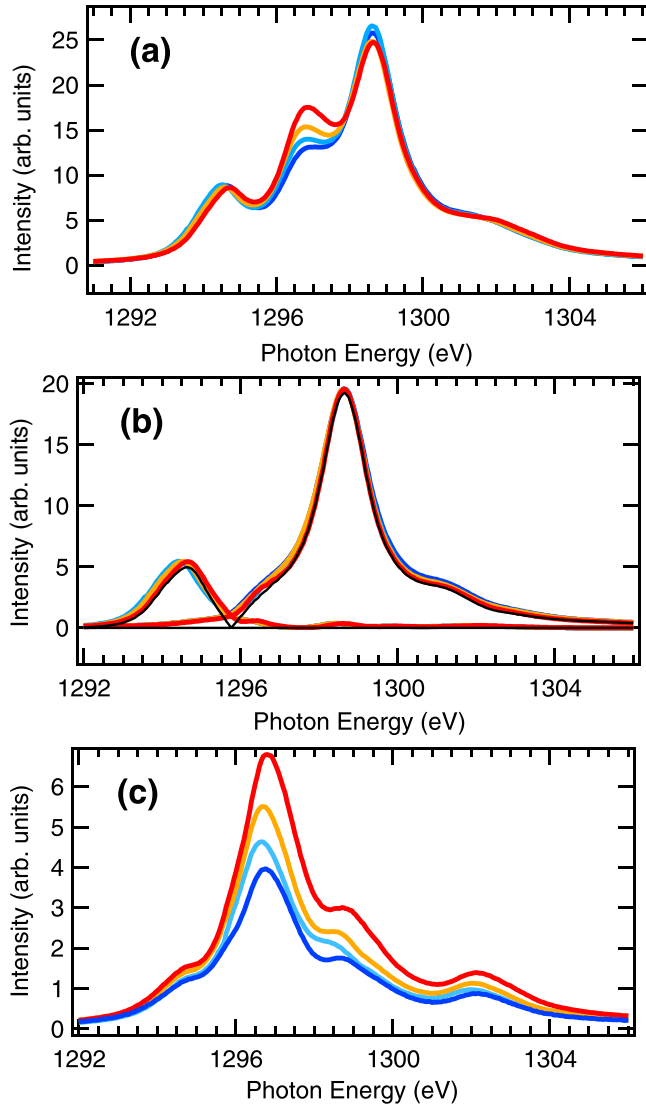


FIG. 8. (a) XAS spectrum ( $C^+ + C^-$ ) of sample DCC taken at 2 K and at different orientation angles:  $0^\circ$  (dark blue line),  $20^\circ$  (light blue line),  $45^\circ$  (orange line), and  $70^\circ$  (red line). (b) PP and AP components, and (c) TR components extracted from the spectra of the DCC sample at 2 K. The colors code is the same as in (a).

taken at  $70^\circ$  clearly has the lowest overlap proportion in its TR component. Then, the PP-AP overlapping region can be extracted by subtracting this TR component to the TR component withdrawn at  $0^\circ$ , the former being conveniently normalized to the intensity of the  $0^\circ$  TR component. This overlapping component is added to the PP and AP components directly extracted from the XMCD spectra obtained at any angle and temperature. The process is then repeated for the extraction of the related TR components, in this way reducing its overlapping portion and approaching the true TR component.

The result of applying this process in our samples is shown in Fig. 8. Although the overall shape of each of the components is very similar for any spectra, they were not exactly the same. For instance, we observed an upward shift in the energy position of the AP peak with respect to the PP peak

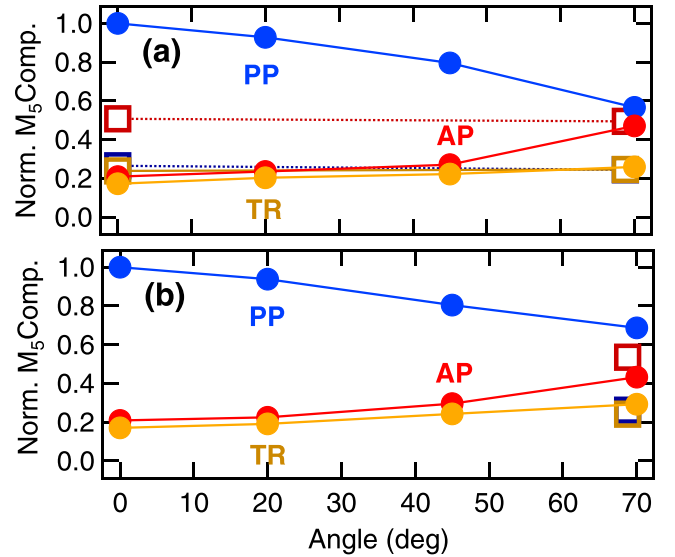


FIG. 9. Normalized PP (blue dots), AP (red dots), and TR (yellow dots) components in Dy  $M_5$  spectra of samples (a) DCC and (b) DCM taken at 2 K as a function of the circularly polarized incident beam. Empty squares are related to the components of the Dy  $M_5$  spectra taken at RT.

with increasing field orientation angle, which is visible in their XAS spectrum shown in Fig. 8(a) for sample DCC. The same effect occurs in sample DCM and at RT. The reason of this is beyond the scope of this paper. More specific experiments are required to determine if these differences, which are small in any case, are caused by experimental factors or because the spectra are actually sensitive to the chemical and/or crystal field environments [21,44,45]. However, such differences imposed that the deconvolution of each spectrum and, later on, its model fitting, had to be done using its own PP, AP, and TR components. We noticed that the obtained coefficients for each of the components used in the deconvolution of the spectra have little variation when using the corrected or the uncorrected spectral components.

## B. Results of the deconvolution of the spectra in the PP, AP, and TR components

Figure 9 shows the normalized coefficients of the three spectral components obtained from the deconvolution of the spectra of the two samples DCC and DCM at RT and 2 K, as a function of the beam and magnetic field orientation angle. The plot was done to compare it with the angle-dependent coefficients plotted in Figs. 6(a) and 6(b), which are cross-section independent. The normalization of the coefficients was done by dividing all the components by the intensity of the PP component measured at normal incidence, which is the one with the highest intensity, and corrected by their relative cross sections. Cross sections were obtained from Ref. [42]. The used cross-section ratio between the PP and the AP components were 3.4, and 1.85 between PP and TR components. The TR component is divided by 2, since there are two possible traversal directions to  $J_z$ .

The coefficients obtained at 2 K had the TR component smaller than the AP component at any angle. There is not

any dysprosium moment orientation with such a coefficient configuration in Fig. 6. The same occurs at RT. In this case, the AP experimental coefficient is notoriously higher than the PP coefficient. Moreover, the PP coefficient reaches such a value only when the dysprosium magnetic moment orientation is in plane. All this means that the dysprosium spectra of the DCC and DCM samples cannot be understood using a single distribution of dysprosium magnetic moments.

This finding supports the conclusion derived from the low magnetic moment value of dysprosium at RT in Sec. III D: the observed spectra must be the result of the combination of the spectra from, at least, two different distribution of dysprosium magnetic moments. One of them must have the dysprosium poorly magnetically coupled or even uncoupled from cobalt. For this to happen, a possibility is to have this dysprosium physically separated from the DyCo alloy by segregation at the interface with the aluminum cap layer.

### C. Description of the model to fit the spectra

RE segregation is a common effect in RE-TM alloys, with the RE always located at the free surface region [17,18,21,22]. Then, the total spectra cannot be built by the simple summation of two spectra. That would be the case if the two types of dysprosium atoms were uniformly distributed all through the depth of the film. When TEY detection is used, the measured spectral intensity is built from the secondary electron current which depends on the depth from where they are emitted. Therefore, the excitations produced at the surface are more heavily weighted than that originating in the layers underneath the segregated dysprosium. For instance, a possible way to explain the larger-than-expected intensity of component AP found in the spectra is by the presence of dysprosium with a low magnetic moment (large cone opening angle) at the topmost surface of the alloy.

The intensity of the secondary electrons collected by the detector depends on the depth from where they are generated by two factors: their escape depth in the excited layers ( $\lambda_e$ ), and the x-ray intensity which is absorbed as it propagates through them. This causes distortions in the measured spectra with respect to the true absorption coefficient of the analyzed sample. These saturation effects become more important as the angle of incidence is increased, because the x-ray penetration depth becomes similar to the secondary electron escape depth [32]. Such effects are taken into account when the spectra are analyzed to recover the absorption coefficients that were originated using a method which is fully described in Ref. [21]. Note that this analysis process assumes the presence of a single layer.

Then, two steps are required to untangle the experimental spectra in their contributions from the different regions at different depths from the film surface. The first step is to model the experimental spectra assuming the presence of, at least, two layers with different thickness, dysprosium concentrations, magnetic moment distributions, and secondary electron escape lengths. The modeling of the spectra is done using the absorption cross section of the PP, AP, and TR components (i.e., the related peak shapes  $A_{JJ'}^{-1}$ ,  $A_{JJ'}^1$ , and  $A_{JJ'}^0$ ), multiplied by their corresponding angle-dependent coefficients calculated from Eq. (3). The sum of the contribution of each layer is

weighted depending on their specific thickness and depth. The resulting spectral intensity follows the expression

$$I(E) \approx \frac{I_{0n}}{\cos \theta_i} \left( \mu_1(E) \frac{(1 - e^{-\frac{z_1}{\lambda_{e1}}})}{\frac{\lambda_{e1}\mu_1(E)}{\cos \theta_i} + 1} + \mu_2(E) \frac{\lambda_{e2}}{\lambda_{e1}} \frac{e^{-\frac{z_1}{\lambda_{e2}}}}{\frac{\lambda_{e2}\mu_2(E)}{\cos \theta_i} + 1} \right). \quad (4)$$

$\theta_i$  is the angle of incidence.  $\mu_i(E)$  is the absorption coefficients of each of the layers, and  $\lambda_{ei}$  is its related electron escape length. This equation has been calculated assuming that the first layer is thinner than the absorption coefficient ( $z \ll \mu_{1,2}(E)$ ), which is applicable in our case.

In the second step, the modeled spectrum passes through the same process as the actual experimental spectrum, described in Ref. [21] to extract what could be called the effective absorption coefficient. This is a necessary step to compare the saturation-corrected experimental effective absorption coefficient, where only a single layer is assumed in the spectrum saturation correction process with the modeled one.

The parameters to enter in the modeling of the spectra are the thickness of the first layer,  $\tau_1$ , the dysprosium concentration  $\rho_i$  of the top layer and the underlayer, the secondary electron escape length  $\lambda_{ei}$  for each of the layers, the overall escape length used to correct saturation effects  $\lambda_{ei}$ , and the opening and inclination angles of the cone of each layer,  $\theta_{Ci}$  and  $\varphi_{Ci}$ . The model that significantly best fitted the spectra required an additional parameter for each layer which represented the portion of dysprosium atoms with moments in the opposite orientation.

Some assumptions were done to choose the value of some of the parameters of the model. The cobalt concentration of the first layer was set to zero in the first layer in the base of the expected RE segregation. The secondary electron escape length was set to 25 Å for both layers. This is the length used in the saturation correction of the experimental spectrum, which was the one that worked the best in these alloys [21]. The validity of this parameter to correct the saturation effects was tested by measuring the experimental ratio between the AP and PP component extracted from the XMCD spectra. This ratio has to be constant for any field orientation and probed sample. Its value was identical to the theoretical one [42] within the experimental error. Different values of the above-mentioned fixed parameters were tried to check the incidence in the results of the fits. Their variation over a relatively wide range of values did not change in a substantial way the conclusions of the spectral fits presented here.

The goodness of the fits were evaluated by minimizing a reduced  $\chi^2$  function,  $\chi^2 = \frac{1}{N} \sum (\frac{y-y_i}{\epsilon_i})^2$ , where  $N$  is the number of points in the spectrum,  $y - y_i$  is the difference between the spectrum and the fit, and  $\epsilon_i$  is the standard deviation of the spectrum data. Given the low noise-to-signal ratios of any of the analyzed spectra, the standard deviation of each of the spectral points was considered equal to 1 for all the spectra. Therefore, the  $\chi^2$  values obtained are only to be compared among the fits presented in this paper.

For instance, the inadequacy of fitting the spectra using a single component was tested. This is shown in Fig. 10. The  $M_5$  spectrum of sample DCC measured at 2 K and normal

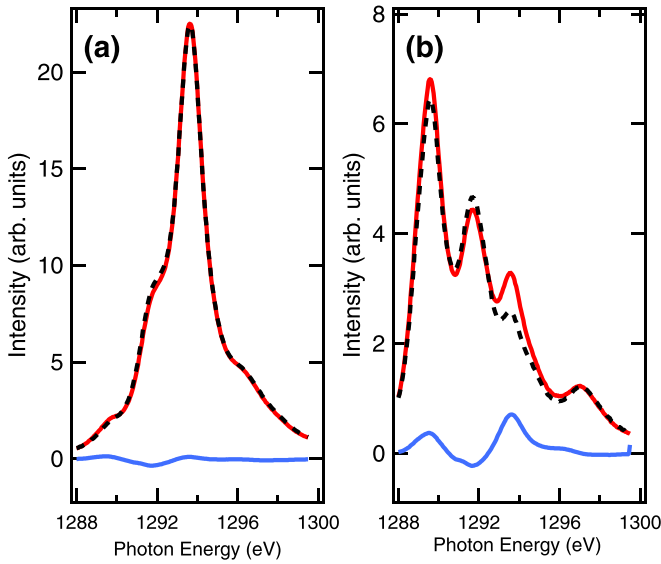


FIG. 10. Fit of the circularly polarized spectra (a)  $C^+$  and (b)  $C^-$  of Dy  $M_5$  of sample DCC taken at 2 K. The red line is the experimental spectrum, the dashed black line is the fitted curve, and the blue line is the residual.

incidence was fitted using a single dysprosium distribution component. The magnetic moment of the distribution used in the fit had the same value as the deduced from the XMCD sum rules. The quality of the fit was visibly lower than the obtained using the two layer model shown in Fig. 13, with a  $\chi^2$  value ten times higher (see Table IV). This confirms the previous conclusion extracted from the deconvolution of the spectra in their PP, AP, and TR components (see Fig. 9). By contrast, Fig. 11 shows the fitting of the circularly polarized spectra of sample DCC at RT an  $0^\circ$  incident angle using the proposed two-layer model as an example of the quality of the fit, with a  $\chi^2$  value ten times smaller than the single layer model. The comparison between the residuals of Figs. 10 and 11 shows that the differences between model and spectrum in the former are concentrated close to certain peaks, whereas these differences seems uniform distributed in the later, demonstrating the fundamental invalidity of a single component model and the meaning of the reduced  $\chi^2$  values for these spectra.

The accuracy of the fitted parameters and the discrimination accuracy of the possible configurations was increased by fitting at the same time the spectra taken at opposite circular polarizations. Both spectra are symmetrical in their spectral components and, therefore, they must use the same fitting parameters: the TR component does not change with circular polarization light and the PP and AP components interchange in the opposite helicity. The magnetic moment obtained from the fits was imposed to be the same as the experimental one.

The spectral fittings were done using the PP and AP components with (corrected) and without (uncorrected) the overlapping component, using the related TR component in each case. We will only show the results corresponding to the corrected components. The results were essentially the same using the uncorrected components.

The analysis of the spectra used two layers for the spectra modeling. Including a larger number of layers might com-

TABLE IV. Fitting parameters of Dy  $M_5$  spectra of samples DCC and DCM taken at RT and 2 K and at different sample orientations with respect to the applied field.  $\tau_1$ : Thickness of the top layer.  $\theta_{C1}$  and  $\theta_{C2}$ : Half-opening cone angle for the fanning distribution of the magnetic moment of dysprosium in the top and under the top probed layers, respectively.  $\varphi_{C2}$ : Cone inclination angle with respect to the beam (field) orientation in the underlayer.;  $m_{C2}$ : Estimated magnetic moment of the underlayer.  $\rho_2$ : Effective atomic concentration of dysprosium at the underlayer. AP<sub>1</sub>: Proportion of antiparallel dysprosium in the first layer (only at 2 K).  $\chi^2$ : Statistical goodness of the fit.

Sample	T	Field orientation angle				
		$0^\circ$	$20^\circ$	$45^\circ$	$70^\circ$	
DCC	RT	$\tau_1$	1.6(1) Å	—	—	1.5(1) Å
		$\theta_{C1}$	$90^\circ$	—	—	$90^\circ$
		$\theta_{C2}$	53.5(1) $^\circ$	—	—	54.1(1) $^\circ$
		AF <sub>C2</sub>	0.26(1)	—	—	0.26(1)
		$m_{C2}$	-3.8(1)	—	—	-3.8(1)
		$\rho_2$	DyCo <sub>3,6(2)</sub>	—	—	DyCo <sub>4,9(3)</sub>
		$\chi^2$	0.6	—	—	0.8
	2 K	$\tau_1$	2.1(1) Å	2.0(1) Å	2.8(1) Å	5.6(1) Å
		$\theta_{C1}$	$90^\circ$	$90^\circ$	$90^\circ$	$90^\circ$
		$\theta_{C2}$	35.9(1) $^\circ$	45.7(2) $^\circ$	47.5(2) $^\circ$	40.2(1) $^\circ$
		$\varphi_{C2}$	0	$10^\circ$	$9^\circ$	$47^\circ$
		$m_{C2}$	8.9	8.2	8.1	5.8
		$\rho_2$	DyCo <sub>5,1</sub>	DyCo <sub>5,0</sub>	DyCo <sub>5,2</sub>	DyCo <sub>5,8</sub>
		AP <sub>1</sub>	56%	64%	56%	39%
$\chi^2$	1.74	3.23	2.0	0.9		
DCM	RT	$\tau_1$	—	—	—	1.5 (1) Å
		$\theta_{C1}$	—	—	—	$90^\circ$
		$\theta_{C2}$	—	—	—	-56.7(1) $^\circ$
		AF <sub>C2</sub>	—	—	—	0.26(1)
		$m_{C2}$	—	—	—	-3.7(1)
		$\rho_2$	—	—	—	DyCo <sub>5,3</sub>
		$\chi^2$	—	—	—	0.4
	2 K	$\tau_1$	2.6(2) Å	2.4(2) Å	3.3(2) Å	3.7(2) Å
		$\theta_{C1}$	$90^\circ$	$90^\circ$	$90^\circ$	$90^\circ$
		$\theta_{C2}$	27.0(1) $^\circ$	32(1) $^\circ$	44(1) $^\circ$	48(1) $^\circ$
		$\varphi_{C2}$	0(1) $^\circ$	6(1) $^\circ$	25(1) $^\circ$	46(1) $^\circ$
		$m_{C2}$	9.3(2)	9.0(2)	7.8(2)	6.1(2)
		$\rho_2$	DyCo <sub>4,9(1)</sub>	DyCo <sub>5,3(1)</sub>	DyCo <sub>5,4(1)</sub>	DyCo <sub>5,4(1)</sub>
		AP <sub>1</sub>	61%	61%	58%	52%
$\chi^2$	3.3	3.3	3	2.8		

promise the accuracy of the analysis due to the consequent increase in the number of variables. Also, the thickness of the effective probed layer, which is estimated to be of the order of 2 to 3 nm, leaves little room for a better in-depth accuracy for the method, because the intensity is exponentially reduced with depth. X-ray photoemission measurements of the samples after the experiment showed a clear larger dysprosium concentration at the surface than that nominally expected. This justified the use of the two-layer model with the topmost layer related to segregated RE. This was also the model that preserved the highest coherence in the obtained parameters of the fits for the variations of temperature, sample, and sample orientation.

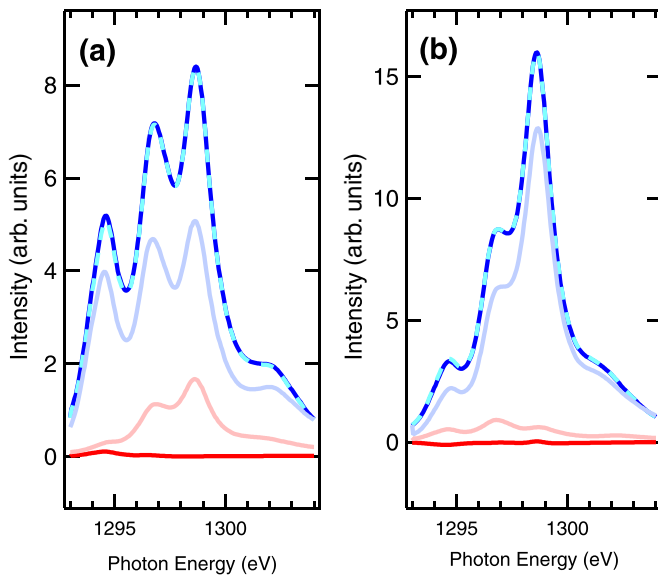


FIG. 11. Fit of the circularly polarized spectra (a)  $C^+$  and (b)  $C^-$  of Dy  $M_5$  of sample DCC taken at RT. The dark blue line is the experimental spectrum, the dashed light blue line is the fitted curve, and the red line is the residual. The light red line is the spectral component for the first layer and the blue line is the spectral component for the underlayer.

#### D. Results and discussion of the fits

Table IV shows the parameters used in the fits with the lowest  $\chi^2$  of the spectra taken at RT and 2 K. The fits are consequent with the main conclusion extracted from the deconvolution of the spectra in their PP, AP, and TR components, shown in Fig. 9. This can be summarized by saying that the intensity of the AP component in the spectra was larger than expected if a single magnetic moment distribution of dysprosium was used. The moment distribution in the two layers model was conditioned by the intensity of this component in the fitted spectra. This is because there are only two ways to get intensity in this peak: either the cone angle of the dysprosium magnetic moment distribution is wide open or it must be oriented in the opposite direction to the main component of the magnetic moment of dysprosium. Note that, in the first case, all the three components, AP, PP, and TR, are excited (see Fig. 6).

To get the low magnetic moment value obtained at RT temperature by XMCD, the system requires a portion of dysprosium with its magnetic moment in the opposite direction to that of the dysprosium AF coupled to cobalt. This explains the large intensity of the AP component in the spectra taken at RT. At 2 K, the AP component should be located at the top layer because, otherwise, it must be admitted the presence of dysprosium ferromagnetically coupled to cobalt or magnetically uncoupled in the underlayer. Then, the RT spectra were fitted using a paramagnetic component ferromagnetically oriented for the top layer, and two dysprosium components opposite oriented for the underlayer, whereas in the 2 K spectra the top layer had two components and the underlayer a single one. This implied a magnetic behavior for the top layer at 2 K that differed from that fitted at RT: the moment distribution

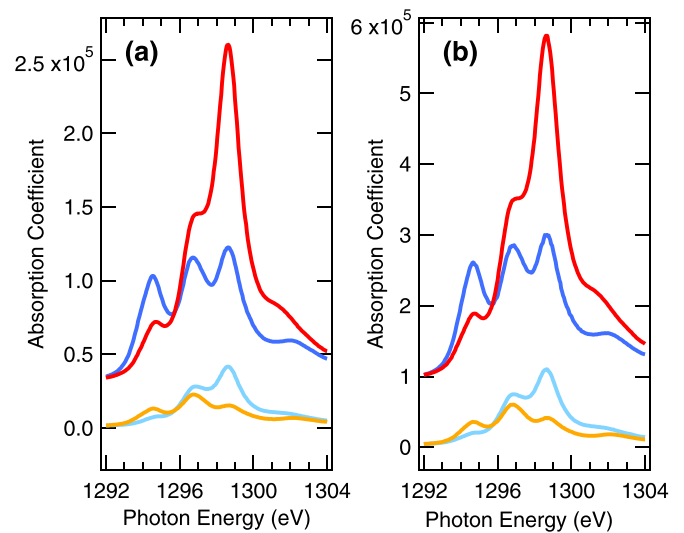


FIG. 12. Spectral components of the Dy  $M_5$  circularly polarized spectra of sample DCC taken at RT and at (a)  $0^\circ$  and (b)  $70^\circ$  orientation field angles. For  $C^+$  polarization, light blue line for the top layer and dark blue line for the under layer. For  $C^-$  polarization, light orange line for the top layer and red line for the underlayer.

for this layer at 2 K caused a reduction of its total moment to almost zero, becoming close to a magnetically dead layer. The presence of some oxidized dysprosium, which is AF below 4 K [46], could explain this effect. The oxidation state does not cause any change in the Dy  $M_{4,5}$  spectra [47] but it does in the Co  $L_{2,3}$  spectra. Cobalt spectra did not show any feature related to oxidized cobalt. This is coherent with the expected location of the possibly oxidized segregated dysprosium, which should be at the interface with the aluminum cap layer.

Figures 12 and 13 show the fitted components for both layers at the two circular polarizations for  $0^\circ$  and  $70^\circ$  incidence angles at RT and 2 K, respectively, and for both samples. The total moment of dysprosium in the underlayer was increased with respect to the nominal deduced from XMCD (Table III) at RT and 2 K as a result of the low magnetic moment of the top layer. At RT, the moment of dysprosium in the underlayer was  $3.8 \mu_B$ , which matched the expected from the VSM data (see Table I) using the cobalt moment deduced from XMCD. At 2 K, the total magnetization of the underlayer, taking the cobalt moment of Table II, was  $349 \text{ emu/cm}^3$  in both samples. This value is several times the value measured by VSM in DCC ( $150 \text{ emu/cm}^3$ ) and DCM ( $100 \text{ emu/cm}^3$ ) samples. This might be explained by assuming a reduced anisotropy at the region probed by TEY, as explained below and the fits of the spectra measured at different orientation angles suggest. XMCD measurements sensitive to the bulk should help to confirm this extreme.

The proportion of dysprosium not AF oriented to cobalt was estimated in 25% of the total. The coupling strength of this dysprosium to cobalt must be either too weak or null and it might be caused by a segregation process and/or by disorder. At low temperature, this type of dysprosium in the underlayer should contribute to increase the total magnetic moment of the dysprosium sublattice. Because of its weak coupling strength to cobalt, this dysprosium that does not contribute to the total

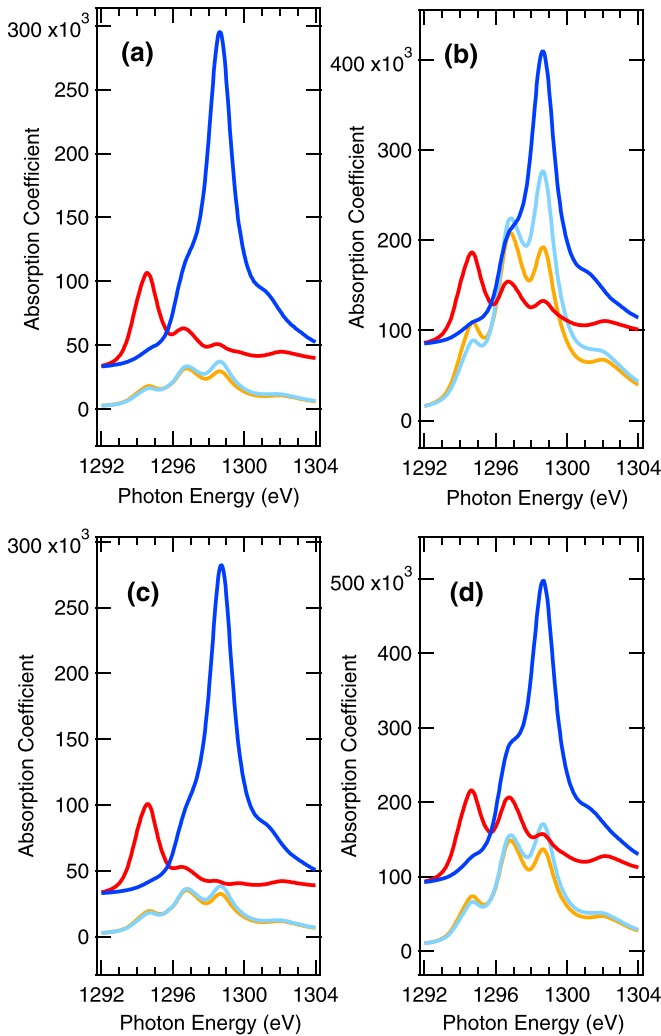


FIG. 13. Spectral components of the circularly polarized spectra  $Dy M_5$  taken at 2 K and at (a)  $0^\circ$  and (b)  $70^\circ$  orientation field angles for sample DCC, and at (c)  $0^\circ$  and (d)  $70^\circ$  for sample DCM. For  $C^+$  polarization, light blue line for the top layer and dark blue line for the underlayer. For  $C^-$  polarization, light orange line for the top layer and red line for the under layer.

magnetic anisotropy of the alloy. It has to also be responsible for the observed small decoupling between the cobalt and dysprosium hysteresis loops (see Sec. III A).

The results of the fits are, therefore, coherent with the expected magnetic behavior of the alloy in the presence of segregated RE, which in the analyzed samples occurs not only in the top layer but also in the underlayer. This explains why dysprosium appears less magnetically anisotropic than cobalt in the analyzed samples when they are measured by TEY. The fits showed, however, some apparent inconsistencies in the values of the thickness of the first layer and the cobalt concentration of the underlayer, which are caused by the limitations in the model used to fit the spectra. These consisted of an increased value of both parameters with the incident angle, indicating that the spectral weight given to the top layer in Eq. (4) was below that required in the fits. The second inconsistency was an increase in the values of these parameters when the temperature decreased to 2 K. These two

effects could be attributed, at least partially, to the simplicity of the model, which does not consider any gradation in the moment distribution from one layer to the other, and to the fact that the spectra represents moment distributions, which might change with the temperature, and not chemical changes.

The thickness values for the top layer used in the fits are small, of the order of one dysprosium monolayer, and its highest value is not higher than two monolayers. These values might not be the actual ones. For instance, they are below the estimated roughness of the film surfaces. Moreover, some diffusion of dysprosium within the aluminum capping layer is expected that should extend the thickness of the top layer of dysprosium, decreasing its density and concentration. These details are not contemplated in the fits, where the concentration of the top layer was fixed to pure dysprosium. Therefore, thickness and concentrations would be acting as effective parameters. This would explain the apparent increase in the thickness of the top layer and/or in cobalt concentration in the underlayer at higher incident angles. In this situation, the signal from the underlayer will be taken from deeper regions, which have lower secondary electrons emitted and a larger path for them to escape up to the surface of the sample. This leads to an increase in the spectral weight of the top layer in the spectra.

However, this cannot fully explain the larger spectral weight of the top layer in the spectra taken at 2 K and  $70^\circ$  angle incidence with respect to the spectra taken at RT. This can be checked by comparing the spectral components used to fit the spectra taken at RT in Fig. 12 with those taken at 2 K shown in Fig. 13. Moreover, the spectral weight of the top layer is different depending on the sample, being especially large in sample DCC, as it can be observed in Fig. 13. The difference of the fitted parameters in these two samples at  $70^\circ$  incidence angle is related to their different intensity in their AP component, as shown in Fig. 14(b). This indicates a different magnetic behavior at 2 K since their spectra at RT was similar.

The apparent persistence of this thicker top layer at 2 K and  $70^\circ$  sample orientation was tested by forcing a reduction in its thickness in the fits to match those at low incidence angles. The result of those fits was discarded because the related magnetic moment values deduced from the fits were below the values measured by XMCD, and they were inconsistent with the values obtained at the other angles.

A plausible explanation for this effect might have to do with the sensitivity of the dysprosium spectrum to the moment distribution across the thickness of the film and not to its chemistry. The magnetization of the probed dysprosium increases from RT to 2 K. Pure dysprosium becomes ferromagnetic at temperatures below 80 K and oxidized dysprosium is AF at temperatures below 4 K. This means that the changes in the orientation of the dysprosium moment should be more gradual from the top layer to the underlayer at 2 K than at RT, as the fits suggest. As the orientation of the applied magnetic field deviates from the easy axis, the top layer with its nearly zero average magnetic momentum would penetrate into the film driven by the increasing energy of the anisotropy field that reduced the magnetization in the direction of the applied field [48]. More measurements done at different temperatures are needed to fully test this explanation, which will

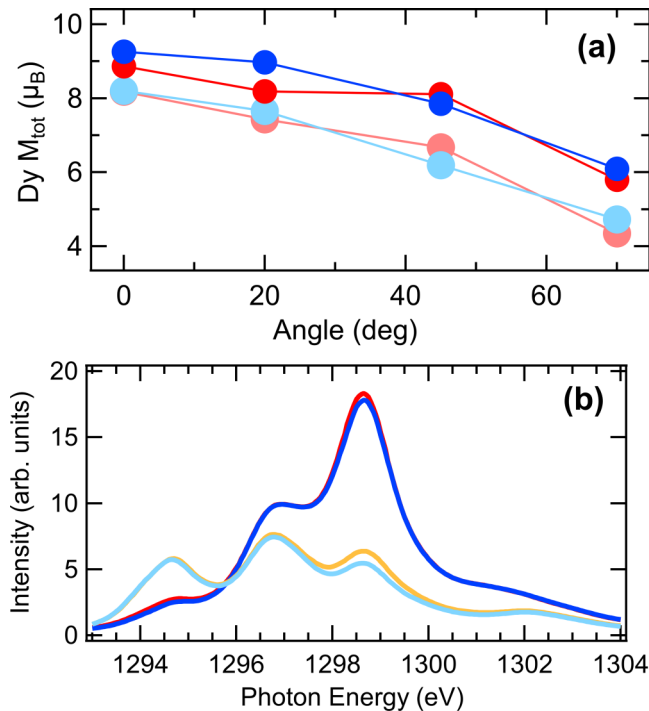


FIG. 14. (a) Comparison between the magnetic moment of dysprosium in the underlayer resulting from the two-layer model fits (red dots, sample DCC; blue dots, sample DCM), and the magnetic moments measured considering a single dysprosium magnetic state as a function of the field orientation angle. (b) Comparison between the spectra of the  $Dy M_5$  circularly polarized spectra of samples DCC and DCM taken at 2 K and at  $70^\circ$ . Dark ( $C^+$ ) and light ( $C^-$ ) blue lines for sample DCM and red ( $C^+$ ) and orange ( $C^-$ ) lines for sample DCC.

definitively prove the high sensitivity of the proposed analysis method to the variations in the magnetic moment of the REs at the region probed by TEY.

## V. CONCLUSIONS

To summarize, the magnetism of the dysprosium and the cobalt sublattices in ferromagnetic DyCo thin films with PMA has been investigated by XMCD spectroscopy using TEY detection. Some unexpected results were observed in the magnetic behavior of the dysprosium sublattice. The measurements done at the Co  $L_{2,3}$  showed that the PMA of the films must stem from the RE sublattice. However, at 2 K, when the PMA energy of the films was the highest, the probed cobalt sublattice resulted to be magnetically more anisotropic than the dysprosium sublattice. Additionally, the magnetic moment of the dysprosium sublattice measured at RT was lower than expected if all moments were AF coupled to cobalt. To understand the cause of these apparent anomalies, a method to analyze the circularly polarized  $Dy M_5$  spectra obtained by TEY has been presented, which is based in the deconvolution of their parallel, antiparallel, and transverse to  $J_z$  spectral components. This spectral analysis reveals the presence of a relatively large proportion of dysprosium with its average moment oriented in the same direction as cobalt, and a thin layer of segregated dysprosium at the top of the alloy which

should not be exchanged coupled to cobalt. Some of the dysprosium in this layer is AF coupled at 2 K, suggesting that either it is partially oxidized or there exist a proportion of dysprosium which is magnetically dead at this temperature. The apparently lower magnetic anisotropy of dysprosium with the field orientation angle is explained by the thickness of the segregated dysprosium layer at the region near the surface. A similar kind of measurement should be conducted using bulk detection sensitivity to determine the precise distribution of RE sites that contribute to the PMA of the alloy. This seems mandatory to be able to predict with accuracy the possible magnetic configurations resulting from the interaction between RE and TM sublattices.

The presented results show that if the RE is segregated at the surface, care must be taken to remove its contribution to the value of the RE magnetic moment measured using TEY detection. This affects, for instance, the  $T_{comp}$  values of RE-TM alloys measured at the surface in this way, which could be overestimated.

The proposed analysis method can serve to detect the presence of RE in different magnetic states, either in the surface or in the bulk. The method can be extended to the circularly polarized spectra of other RE at the  $M_{4,5}$  edge, whenever the angular momentum  $L$  of its  $4f$  orbital is different of zero (i.e., it could not be applied to  $Gd^{+3}$ ). In those other RE, the identification of the PP, AP, and TR spectral components requires a different methodology than that presented here for dysprosium since their overlap is much important. This might not be a problem because these components are well approximated by theory. Better, they could be isolated by spectroscopic methods using circular but also linear polarized spectroscopy at the related RE  $M_{4,5}$  edges. Nevertheless, more additional work is needed to improve and test the accuracy of the method by better characterizing the region probed with other surface-sensitive techniques.

The experiment confirms the presence of segregated RE reported in other RE-TM systems. The preparation method of the alloy did not produce substantial differences in the magnetism of the cobalt and dysprosium sublattices at the surface of the alloy, indicating that the origin of their different macroscopic behaviors has to be found in the bulk or they are caused by their different microstructures. The nondependence of the RE segregation with the deposition method (cosputtering and alternate deposition) remarks that the segregated RE is an immediate postdeposition process, which can proceed during time as has been observed in GdCo [17]. This is also demonstrated in the DCM film whose last deposited layer, before depositing the aluminum capping layer, was cobalt. This means that RE atoms could also diffuse in the bulk at defects like voids, cracks, and grain borders within the bulk. This might affect magnetic properties like, for instance, the coercive field of the thin films.

## ACKNOWLEDGMENTS

J.D. acknowledges M. Valvidares for BOREAS beamline set up and his help in the beamline during data acquisition, and C. Quirós, and J. M. Alameda for providing the samples and the VSM measurements. This project has been supported by Spanish MICINN under Grants

No. FIS2016-76058 (AEI/FEDER, EU) and No. PID2019-104604RB/AEI/10.13039/501100011033.

### APPENDIX: ORIENTATION DEPENDENCE OF LIGHT ABSORPTION

This Appendix shows the details of the calculation of the intensity absorbed by circularly polarized light when the orientation of the angular momentum of the  $4f$  orbital forms an angle  $\theta$  with the direction of the wave vector  $\vec{k}$  which is chosen parallel to the  $z$  axis. The components of the electric field of the circularly polarized light in the frame of the  $4f$  angular momentum, with its  $z_m$  axis along its quantization axis, are calculated by making a first rotation of an angle  $\varphi$  in the  $xy$  polarization plane ( $z$  axis as the rotation axis) followed by a rotation of an angle  $\theta$  around the resulting  $y$  axis after the first rotation:

$$\begin{pmatrix} \epsilon_{x_m} \\ \epsilon_{y_m} \\ \epsilon_{z_m} \end{pmatrix} = \begin{pmatrix} \cos \varphi & -\sin \varphi & 0 \\ \sin \varphi & \cos \varphi & 0 \\ 0 & 0 & 1 \end{pmatrix} \begin{pmatrix} \cos \theta & 0 & -\sin \theta \\ 0 & 1 & 0 \\ \sin \theta & 0 & \cos \theta \end{pmatrix} \begin{pmatrix} \epsilon_x \\ \epsilon_y \\ \epsilon_z \end{pmatrix}. \quad (\text{A1})$$

Therefore, for right ( $-$ ) and left ( $+$ ) circular polarization:

$$\begin{pmatrix} \epsilon_{x_m} \\ \epsilon_{y_m} \\ \epsilon_{z_m} \end{pmatrix} = \frac{\epsilon e^{\pm i\varphi}}{\sqrt{2}} \begin{pmatrix} \cos \theta \\ \mp i \\ \sin \theta \end{pmatrix}. \quad (\text{A2})$$

By using this result, the electric dipole operator  $P$  written in the frame of the  $4f$  orbital read

$$P = \frac{e^{\pm i\varphi}}{\sqrt{2}} [P_{x_m}^0 \cos \theta \mp iP_{y_m}^0 + P_{z_m}^0 \sin \theta]. \quad (\text{A3})$$

The superscript in the dipole operator indicates the polarization state of the electric field in the frame of the  $4f$  orbital: 0 is lineal, 1 left circular, and  $+1$  right circular. The electric dipole operator can be expressed in the components parallel to the quantization axis  $z_m$  of the  $4f$  orbital using the

relations

$$P_{x_m}^0 = \frac{1}{\sqrt{2}} [P_{z_m}^{-1} + P_{z_m}^1] \quad (\text{A4})$$

and

$$P_{y_m}^0 = \frac{i}{\sqrt{2}} [P_{z_m}^{-1} - P_{z_m}^1]. \quad (\text{A5})$$

Then

$$P = \frac{e^{\pm i\varphi}}{\sqrt{2}} \left[ \frac{(\cos \theta \pm 1)}{\sqrt{2}} P_{z_m}^{-1} + \frac{(\cos \theta \mp 1)}{\sqrt{2}} P_{z_m}^1 + P_{z_m}^0 \sin \theta \right]. \quad (\text{A6})$$

The absorption cross section for the excitation from a state  $|\alpha m J\rangle$  to a state  $|\alpha' m' J'\rangle$  is, in the dipole approximation,

$$\sigma_{\alpha m J \rightarrow \alpha' m' J'} = 4\pi^2 \alpha_0 \hbar \omega |\langle \alpha m J | P | \alpha' m' J' \rangle|^2. \quad (\text{A7})$$

The cross section for circular polarized light is obtained substituting Eq. (1) in Eq. (2),

$$\sigma_{\alpha m J \rightarrow \alpha' m' J'} = 4\pi^2 \alpha_0 \hbar \omega S_{\alpha J \alpha' J'} \left[ \frac{(\cos \theta \pm 1)^2}{4} A_{J J'}^{-1} + \frac{(\cos \theta \mp 1)^2}{4} A_{J J'}^1 + \frac{\sin^2 \theta}{2} A_{J J'}^0 \right], \quad (\text{A8})$$

where  $S_{\alpha J \alpha' J'}$  is the radial integer and  $A_{J J'}^q$  are the angular integers. Under the assumption of a weak crystal field, as happens in dysprosium, the values of the radial and angular integers do not change. Only the relative orientation of the moment with respect to incident beam changes. We redefine the angular integers as the absorption cross sections for the corresponding situation in which the polarized beam and the magnetization are parallel ( $q = 0, \pm 1$ ). Then, the  $\theta$ -dependent functions that multiply to each of the related  $q = 0, \pm 1$  cross sections are the coefficients for the TR ( $q = 0$ ), PP ( $q = -1$ ) and AP ( $q = +1$ ) components:

$$\begin{aligned} &PP + AP + TR \\ &= \left[ \frac{(\cos \theta \pm 1)^2}{4} A_{J J'}^{-1} + \frac{(\cos \theta \mp 1)^2}{4} A_{J J'}^1 + \frac{\sin^2 \theta}{2} A_{J J'}^0 \right]. \end{aligned} \quad (\text{A9})$$

[1] K. H. J. Buschow, Intermetallic compounds of rare-earth and 3d transition metals, *Rep. Prog. Phys.* **40**, 1179 (1977).  
[2] R. Skomski and D. Sellmyer, Anisotropy of rare-earth magnets, *J. Rare Earths* **27**, 675 (2009).  
[3] C. Blanco-Roldán, Y. Choi, C. Quirós, S. M. Valvidares, R. Zarate, M. Vélez, J. M. Alameda, D. Haskel, and J. I. Martín, Tuning interfacial domain walls in GdCo/Gd/GdCo' spring magnets, *Phys. Rev. B* **92**, 224433 (2015).  
[4] R. Morales, J. I. Martín, and J. M. Alameda, Domain walls and macroscopic spin-flip-like metamagnetism in  $\text{Gd}_x\text{Co}_{1-x}/\text{G}_y\text{Co}_{1-y}$  exchange-coupled double layers, *Phys. Rev. B* **70**, 174440 (2004).  
[5] K. Chen, D. Lott, F. Radu, F. Choueikani, E. Otero, and P. O. Observation of an atomic exchange bias effect in DyCo<sub>4</sub> film, *Sci. Rep.* **5**, 18377 (2015).

[6] C. Blanco-Roldán, C. Quirós, A. Sorrentino, A. Hierro-Rodríguez, L. M. Álvarez-Prado, R. Valcárcel, M. Duch, N. Torras, J. Esteve, J. I. Martín, M. Vélez, J. M. Alameda, P. E., and S. Ferrer, Nanoscale imaging of buried topological defects with quantitative x-ray magnetic microscopy, *Nat. Commun.* **6**, 8196 (2015).  
[7] L. Caretta, M. Mann, F. Büttner, K. Ueda, B. Pfau, C. M. Günther, P. Hessing, A. Churikova, C. Klose, M. Schneider, D. Engel, C. Marcus, D. Bono, K. Bagschik, S. Eisebitt, and G. S. D. Beach, Fast current-driven domain walls and small skyrmions in a compensated ferrimagnet, *Nat. Nanotech.* **13**, 1154 (2018).  
[8] A. Hierro-Rodríguez, C. Quirós, A. Sorrentino, L. M. Alvarez-Prado, J. I. Martín, J. M. Alameda, S. McVitie, E. Pereiro, M. Vélez, and S. Ferrer, Revealing 3d magnetization of thin



- films with soft x-ray tomography: Magnetic singularities and topological charges, *Nat. Commun.* **11**, 6382 (2020).
- [9] D. Markó, F. Valdés-Bango, C. Quirós, A. Hierro-Rodríguez, M. Vélez, J. I. Martín, J. M. Alameda, D. S. Schmool, and L. M. Alvarez-Prado, Tunable ferromagnetic resonance in coupled trilayers with crossed in-plane and perpendicular magnetic anisotropies, *Appl. Phys. Lett.* **115**, 082401 (2019).
- [10] S. Mangin, M. Gottwald, C-H. Lambert, D. Steil, V. Uhlř, L. Pang, M. Hehn, S. Alebrand, M. Cinchetti, G. Malinowski, Y. Fainman, M. Aeschlimann, and E. E. Fullerton, Engineered materials for all-optical helicity-dependent magnetic switching, *Nat. Mater.* **13**, 286 (2014).
- [11] C. Schubert, A. Hassdenteufel, P. Matthes, J. Schmidt, M. Helm, R. Bratschitsch, and M. Albrecht, All-optical helicity dependent magnetic switching in an artificial zero moment magnet, *Appl. Phys. Lett.* **104**, 082406 (2014).
- [12] J. Becker, A. Tsukamoto, A. Kirilyuk, J. C. Maan, T. Rasing, P. C. M. Christianen, and A. V. Kimel, Ultrafast Magnetism of a Ferrimagnet Across the Spin-Flop Transition in High Magnetic Fields, *Phys. Rev. Lett.* **118**, 117203 (2017).
- [13] K. Hummler and M. Fähnle, Full-potential linear-muffin-tin-orbital calculations of the magnetic properties of rare-earth-transition-metal intermetallics. I. Description of the formalism and application to the series RCo<sub>5</sub> (R=rare-earth atom), *Phys. Rev. B* **53**, 3272 (1996).
- [14] J. Stöhr, Exploring the microscopic origin of magnetic anisotropies with X-ray magnetic circular dichroism (XMCD) spectroscopy, *J. Magn. Magn. Mater.* **200**, 470 (1999).
- [15] S. P. Collins, D. Laundy, C. C. Tang, and G. van der Laan, An investigation of uranium M<sub>4,5</sub> edge magnetic x-ray circular dichroism in US, *J. Phys.: Condens. Matter* **7**, 9325 (1995).
- [16] Y. Teramura, A. Tanaka, B. Thole, and T. Jo, Effect of Coulomb interaction on the x-ray magnetic circular dichroism spin sum rule in rare earths, *J. Phys. Soc. Jpn.* **65**, 3056 (1996).
- [17] N. Berggaard, A. Mougín, M. Izquierdo, E. Fonda, and F. Sirotti, Correlation between structure, electronic properties, and magnetism in Co<sub>x</sub>Gd<sub>1-x</sub> thin amorphous films, *Phys. Rev. B* **96**, 064418 (2017).
- [18] E. Haltz, R. Weil, J. Sampaio, A. Pointillon, O. Rousseau, K. March, N. Brun, Z. Li, E. Briand, C. Bachelet, Y. Dumont, and A. Mougín, Deviations from bulk behavior in TbFe(Co) thin films: Interfaces contribution in the biased composition, *Phys. Rev. Materials* **2**, 104410 (2018).
- [19] L. Baczewski, D. Givord, J. Alameda, B. Dieny, J. Nozieres, J. Rebouillat, and J. Prejean, Magnetism in rare-earth-transition metal systems. magnetization reversal and ultra-high susceptibility in sandwiched thin films based on rare-earth and cobalt alloys, *Acta Phys. Pol. A* **83**, 629 (1993).
- [20] C. Luo, H. Ryll, C. Back, and F. Radu, X-ray magnetic linear dichroism as a probe for non-collinear magnetic state in ferrimagnetic single layer exchange bias systems, *Sci. Rep.* **9**, 18169 (2019).
- [21] R. Cid, J. M. Alameda, S. M. Valvidares, J. C. Cezar, P. Bencok, N. B. Brookes, and J. Díaz, Perpendicular magnetic anisotropy in amorphous Nd<sub>x</sub>Co<sub>1-x</sub> thin films studied by x-ray magnetic circular dichroism, *Phys. Rev. B* **95**, 224402 (2017).
- [22] J. Díaz, R. Cid, A. Hierro, L. M. Álvarez-Prado, C. Quirós, and J. M. Alameda, Large negative thermal expansion of the Co sub-network measured by EXAFS in highly disordered Nd<sub>1-x</sub>Cox thin films with perpendicular magnetic anisotropy, *J. Phys.: Condens. Matter* **25**, 426002 (2013).
- [23] M. D. Davydova, K. A. Zvezdin, J. Becker, A. V. Kimel, and A. K. Zvezdin, *h-t* phase diagram of rare-earth-transition-metal alloys in the vicinity of the compensation point, *Phys. Rev. B* **100**, 064409 (2019).
- [24] K. Chen, D. Lott, F. Radu, F. Choueikani, E. Otero, and P. Ohresser, Temperature-dependent magnetic properties of ferrimagnetic DyCo<sub>3</sub> alloy films, *Phys. Rev. B* **91**, 024409 (2015).
- [25] C. Quirós, I. Popa, O. Robach, D. Wermeille, J. Díaz, R. Felici, and S. Ferrer, Stacking dependent disordering processes in Gd/Co/Pt(111) studied with surface x-ray diffraction, *Phys. Rev. B* **78**, 195406 (2008).
- [26] A. Barla, J. Nicolás, D. Cocco, S. M. Valvidares, J. Herrero-Martín, P. Gargiani, J. Moldes, C. Ruget, E. Pellegrin, and S. Ferrer, Design and performance of BOREAS, the beamline for resonant x-ray absorption and scattering experiments at the ALBA synchrotron light source, *J. Synchrotron Radiat.* **23**, 1507 (2016).
- [27] C. Blanco-Roldán, Magnetic interactions in rare earth-transition metal systems and their study by synchrotron radiation techniques PhD thesis, Universidad de Oviedo, 2017.
- [28] L. H. Bennett and E. Della Torre, Analysis of wasp-waist hysteresis loops, *J. Appl. Phys.* **97**, 10E502 (2005).
- [29] M. V. Sapozhnikov, Y. V. Petrov, N. S. Gusev, A. G. Temiryazev, O. L. Ermolaeva, V. L. Mironov, and O. G. Udalov, Artificial dense lattices of magnetic skyrmions, *Materials* **13**, 99 (2020).
- [30] M. Altarelli, Orbital-magnetization sum rule for x-ray circular dichroism: A simple proof, *Phys. Rev. B* **47**, 597 (1993).
- [31] P. Carra, B. T. Thole, M. Altarelli, and X. Wang, X-Ray Circular Dichroism and Local Magnetic Fields, *Phys. Rev. Lett.* **70**, 694 (1993).
- [32] R. Nakajima, J. Stöhr, and Y. U. Idzerda, Electron-yield saturation effects in L-edge x-ray magnetic circular dichroism spectra of Fe, Co, and Ni, *Phys. Rev. B* **59**, 6421 (1999).
- [33] C. T. Chen, Y. U. Idzerda, H.-J. Lin, N. V. Smith, G. Meigs, E. Chaban, G. H. Ho, E. Pellegrin, and F. Sette, Experimental Confirmation of the X-Ray Magnetic Circular Dichroism Sum Rules for Iron and Cobalt, *Phys. Rev. Lett.* **75**, 152 (1995).
- [34] J. Stöhr and H. König, Determination of Spin-and Orbital-Moment Anisotropies in Transition Metals by Angle-Dependent X-Ray Magnetic Circular Dichroism, *Phys. Rev. Lett.* **75**, 3748 (1995).
- [35] G. Van Der Laan, Microscopic origin of magnetocrystalline anisotropy in transition metal thin films, *J. Phys.: Condens. Matter* **10**, 3239 (1998).
- [36] Y. Suzuki and S. Miwa, Magnetic anisotropy of ferromagnetic metals in low-symmetry systems, *Phys. Lett. A* **383**, 1203 (2019).
- [37] C. H. Wu and Y. C. Chuang, The Co-Y (cobalt-yttrium) system, *J. Phase Equilib.* **12**, 587 (1991).
- [38] H. Okamoto, Supplemental Literature Review of Binary Phase Diagrams: Ag-Ho, Ag-Tb, Ag-Y, Cd-Na, Ce-Sn, Co-Dy, Cu-Dy, Cu-Sn, Ir-Pt, Mg-Pb, Mo-Ni, and Sc-Y, *J. Phase Equilib. Diffus.* **35**, 208 (2014).

- [39] J. M. D. Coey, Magnetism in amorphous solids, in *Amorphous Solids and the Liquid State*, edited by N. H. March, R. A. Street, and M. P. Tosi (Springer US, Boston, MA, 1985), pp. 433–466.
- [40] C. E. Patrick and J. B. Staunton, Rare-earth/transition-metal magnets at finite temperature: Self-interaction-corrected relativistic density functional theory in the disordered local moment picture, *Phys. Rev. B* **97**, 224415 (2018).
- [41] B. T. Thole, G. van der Laan, J. C. Fuggle, G. A. Sawatzky, R. C. Karnatak, and J.-M. Esteve, 3d x-ray-absorption lines and the  $3d^9 4f^{n+1}$  multiplets of the lanthanides, *Phys. Rev. B* **32**, 5107 (1985).
- [42] J. Goedkoop, *X-Ray Dichroism of Rare Earth Materials* (Krips Repro, Meppel, 1989).
- [43] J. B. Goedkoop, B. T. Thole, G. van der Laan, G. A. Sawatzky, F. M. F. de Groot, and J. C. Fuggle, Calculations of magnetic x-ray dichroism in the 3d absorption spectra of rare-earth compounds, *Phys. Rev. B* **37**, 2086 (1988).
- [44] G. van der Laan, E. Arenholz, A. Schmehl, and D. G. Schlom, Weak anisotropic x-ray magnetic linear dichroism at the Eu  $M_{4,5}$  edges of ferromagnetic EuO(001): Evidence for  $4f$ -state Contributions, *Phys. Rev. Lett.* **100**, 067403 (2008).
- [45] B. Das, R. Choudhary, R. Skomski, B. Balasubramanian, A. K. Pathak, D. Paudyal, and D. J. Sellmyer, Anisotropy and orbital moment in Sm-Co permanent magnets, *Phys. Rev. B* **100**, 024419 (2019).
- [46] K. P. Shinde, V. M. Tien, L. Huang, H.-R. Park, S.-C. Yu, K. C. Chung, and D.-H. Kim, Magnetocaloric effect in Tb<sub>2</sub>O<sub>3</sub> and Dy<sub>2</sub>O<sub>3</sub> nanoparticles at cryogenic temperatures, *J. Appl. Phys.* **127**, 054903 (2020).
- [47] N. A. Anderson, Q. Zhang, M. Hupalo, R. A. Rosenberg, J. W. Freeland, M. C. Tringides, and D. Vaknin, Magnetic properties of Dy nano-islands on graphene, *J. Magn. Magn. Mater.* **435**, 212 (2017).
- [48] J. M. Tonnerre, M. De Santis, S. Grenier, H. C. N. Tolentino, V. Langlais, E. Bontempi, M. García-Fernández, and U. Staub, Depth Magnetization Profile of a Perpendicular Exchange Coupled System by Soft-X-Ray Resonant Magnetic Reflectivity, *Phys. Rev. Lett.* **100**, 157202 (2008).